Silicon Photomultiplier Classification of the Pre-Production GCT Camera of CTA

Silicon Photomultiplier Klassifikation der Pre-Production GCT Kamera von CTA

Master-Thesis von Ben Gebhardt aus Heidelberg

Tag der Einreichung:

1. Gutachten: Dr. Richard White (MPIK)
2. Gutachten: Prof. Jim Hinton (MPIK)
3. Gutachten: Prof. Tetyana Galatyuk (TU DA)

TECHNISCHE UNIVERSITÄT DARMSTADT

Fachbereich Physik
Max Planck Institut f"ur Kernphysik Heidelberg

Silicon Photomultiplier Classification of the Pre-Production GCT Camera of CTA
Silicon Photomultiplier Klassifikation der Pre-Production GCT Kamera von CTA

Vorgelegte Master-Thesis von Ben Gebhardt aus Heidelberg

1. Gutachten: Dr. Richard White (MPIK)
2. Gutachten: Prof. Jim Hinton (MPIK)
3. Gutachten: Prof. Tetyana Galatyuk (TU DA)

Tag der Einreichung:

Bitte zitieren Sie dieses Dokument als:
URN: urn:nbn:de:tuda-tuprints-12345
URL: http://tuprints.ulb.tu-darmstadt.de/1234

Dieses Dokument wird bereitgestellt von tuprints,
E-Publishing-Service der TU Darmstadt
http://tuprints.ulb.tu-darmstadt.de
tuprints@ulb.tu-darmstadt.de

Erklärung zur Master-Thesis

Hiermit versichere ich, die vorliegende Master-Thesis ohne Hilfe Dritter nur mit den angegebenen Quellen und Hilfsmitteln angefertigt zu haben. Alle Stellen, die aus Quellen entnommen wurden, sind als solche kenntlich gemacht. Diese Arbeit hat in gleicher oder ähnlicher Form noch keiner Prüfungsbehörde vorgelegen.

Darmstadt, den April 10, 2017

(B. Gebhardt)

Contents

Abstract

whats this about

Abstract

worum es geht

1 Introduction

What can we learn by observing gamma rays?

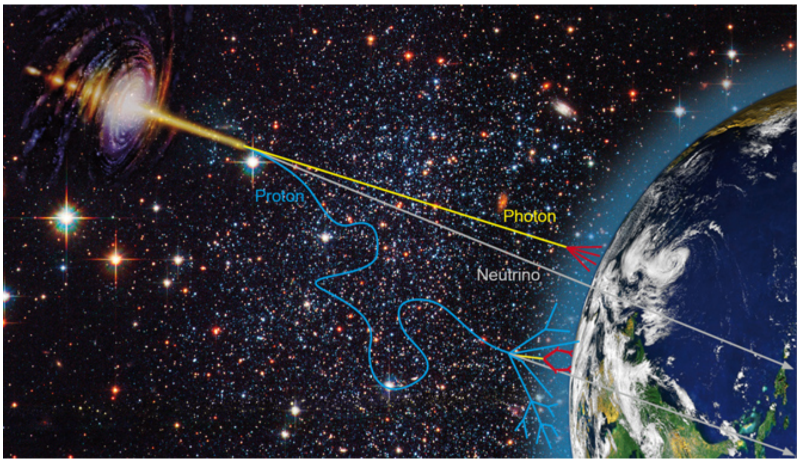

Figure 1: Gamma Radiation and cosmic rays from an astrophysical source arriving on earth.

Gamma radiation cannot be generated by thermal emission of hot stellar objects, the only event with a high enough temperature to produce thermal radiation in the range of GeV and TeV gamma radiation would be the big bang, there is and has been nothing else in the known universe. So, if thermal radiation reflects the temperature of the emitting body, what do gamma rays tell us?

Figure 2: FermiLAT

Gamma radiation probe a non-thermal universe. In this you need other mechanisms to concentrate large amounts of energy into a single quantum. But what are those?
There are many diverse mechanisms of emitting gamma radiation. In short gamma rays are generated by high relativistic particles, in a first step for example: accelerated by the shockwave of a supernova explosion. Those then collide with ambient gas, interact with photons or magnetic fields, by inverse compton scattering. One such supernova remnant and also the most famous, while also being the, to date highest in energy is the Crab Pulsar. The Neutron Star located inside the Crab Nebula is the remnant of Supernova1054 and emits gamma radiation energies up to 80TeV. The source of the gamma radiation here is the so called Pulsar Wind Nebula. It is composed of highly relativistic charged particles from the pulsar interacting with the expanding Supernova remnant via inverse compton scattering. So just like thermal radiation reflects the temperature of the emitting object, the flux and energy spectrum of the gamma rays reflect the flux and spectrum of the high energy particles. So they can be used to trace these comsic rays and electrons in distant regions of our own galaxy or even beyond. Even higher energy gamma

rays could also be the product of decays of heavy particles, like dark matter or cosmic strings. They therefore also provide a window to the discovery of dark matter.

The only problem is, our atmosphere is opaque for gamma radiation, gamma ray astronomy was mainly done by satellite based instruments like FermiLAT. The Large Area Telescope, the principle scientific instrument on the Fermi Gamma-Ray Space Telescope Spacecraft, launched in June 2008. fig (**??**)

2 Silicon Photomultipliers

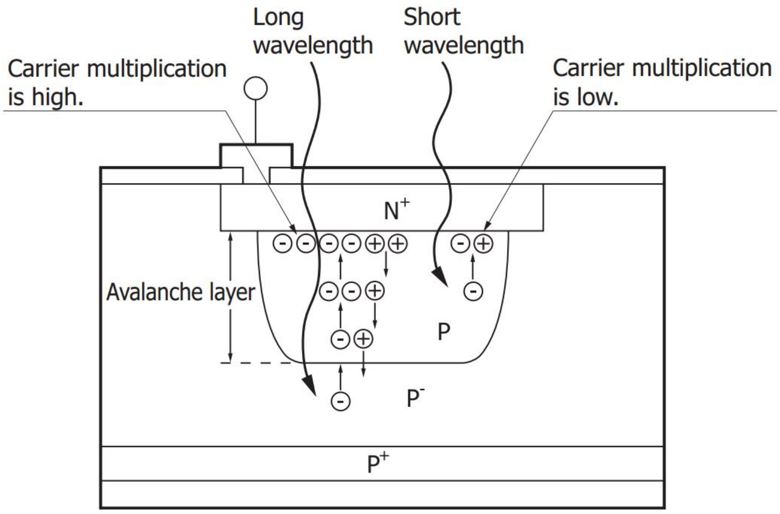

Figure 3:

Silicon Photomultipliers are semiconductor photo detectors, that have attracted increased attention over the last decade for their possible use in astroparticle physics. The sensor consists of an array of avalanche photo-diodes, typically 50μm in size. Depending on the pixel-size, one pixel contains several 1000 diodes, hereafter called cells. Each cell is a PN junction supplied with a reverse bias-voltage above breakdown, which is called operation in Geiger-mode, in analogy to the Geiger counter. In this mode, a photon or thermal excitation will produce an electron-hole pair in the depleted region. Through impact ionization these charge carriers will in turn trigger an avalanche in a cell, which in turn generates a large output pulse typically in the range of several Mega electronvolt. This avalanche is then passively quenched by a resistor to limit the current in the substrate and to reset the cell to a quiet state so it is photosensitive again. The signal of the SiPM is the sum of the signal of all cells, read out over their quenching resistor via a common output.

Silicon Photomultipliers posses major advantages over their progenitor, the Multi Anode Photomultipliertubes, or MAPM. They are more resistent to mechanical and accidental light-exposure damage through ambient light. Silicon Photomultipliers have a lower power consumption and, operating at a much lower bias-voltage, there is no need for high-voltage as in Photomultipliertubes. They posses a high photon detection efficiency and are insensitive to magnetic field changes. There is rapid improvement, being a fairly new technology, with new generations every $\sim$5 months and decreasing costs per mm^2. Viewed over all cells of the whole pixel, fluctuations in the gain are very small. This is because of the uniformity during manufacture and visible in the width and the clear resolution of the p.e. peaks in the pulse area spectrum. **??**. Multi anode photomultipliertubes do not posses those small gain fluctuations, which is due to their structure. These make Silicon Photomultipliers an interesting candidate in astrophysics experiments for both, space- and ground-based telescopes (or IACTs, Imaging Atmospheric Cherenkov Telescopes).

1. Sturdiness
2. May be exposed to ambient light (observation during bright moonlight periods possible)
3. Low power consumption ($\leq 50\mu$W/mm^2)
4. Low operation voltage (typically $\sim$20 - 100 Volts)
5. No need for HV, as in PMTs
6. High Photon detection efficiency
7. Insensitivity to magnetic fields
8. Being a fairly new technology it is steadily improved, meaning a new generation of SiPMs every 5months
9. Rapidly decreasing cost per mm^2

The currently most challenging astrophysics experiment Silicon Photomultipliers are considered for is use in Cherenkov telescopes, with very demanding expectations in terms of photon detection efficiency. The photon detection efficiency quantifies the absolute efficiency of any photon detector to absorb a photon and produce a measurable signal at its output. To achieve a high photon detection efficiency in the 450nm regime, the design moves to very thin implantation layers on the surface in order to minimize the absoprion of shorter wavelength photons in insensitive areas. Figure(**??**) Different entry window coatings and avalanche structures (trenches etc.) explore the capable enhancements in the blue sensitive UV region.

2.1 Gain of a Silicon Photomultiplier

The gain of a Silicon Photomultiplier measures the internal conversion of a photon incident into a signal at the output. The amplification of the device is expressed as the average number of charge carriers produced. There is no distinction weather the incident was caused by a single original photon or a thermal electron.
Estimation can be done via the voltage mean of the 1 p.e. amplitude: (e.g. see Figure (**??**)). For a better understanding, stating the gain in units of mV per photoelectron or $\frac{mV}{p.e.}$ is more suitable, as it gives a direct correlation between detected photoelectron and expected voltage amplitude. Given the very narrow pulse shapes, using the average pulse amplitude and extracting FWHM as a time measure of the total charge flowing during discharge and using the formula:
The gain is obviously higher the larger the cell capacitance or the higher the bias-voltage (eq **??**) will be. But increasing the bias-voltage also increases dark counts and crosstalk. The gain is also

$$
\begin{aligned}
M =& \frac{Q}{e} \\
Q =& C * (V_{bias} - V_{breakdown})
\end{aligned} \tag{1}
$$

Figure 4: The gain (M) of a Silicon Photomultiplier results form the deposited charge (Q) of the pulse generated from one cell when it detects one photon, devided by the charge per electron (e). The charge deposited per event is proportional to the cells capacitance (C) and the supplied over-voltage ($V_{bias} - V_{breakdown}$). This results in the gain (M) in units of total number of charge carriers, usually in the several 10^6 range.

$$
\begin{aligned}
Q(p.e.) =& C * (V_{bias} - V_{breakdown}) \\
U(p.e.) =& \frac{Q(p.e.)}{t(FWHM)} * 50ohm
\end{aligned} \tag{2}
$$

Figure 5: Resulting in the expected event charge flowing during capacitor discharge. Given the bias-voltage and C as capacitance of one cell, a conversion factor and the average amplitude per photoelectron can be extracted.

dependent on the temperature, mainly through the quenching resistor but also from the silicon bulk itself, at a certain bias-voltage decreasing as temperature rises. The quenching resistor is affected by a lowering of the electrical conductivity with rising temperature, in accordance to the WiedemannâĂŞFranz law, stating that the ratio of electrical and thermal conductivity remains constant. The silicon bulk at rising temperatures underlies increased crystal lattice movement. This impinges charge transport by increasing the probability that carriers might impact on the lattice before the carrier energy has become large enough for continued ionization. In order to counteract this, the electric field must be increased by increasing the supplied bias-voltage so ionization is more likely. Doing this has drawbacks as discussed before. For application as a photon detector, keeping the gain constant is an inevitable step, otherwise the shifting gain leads to problems. To do that, either the bias-voltage need to be asjusted to match ambient temperature, leading to problems with varying dark counts and crosstalk. Or the surface temperature must be regulated to be kept constant. Although more challenging hardware would be required, the latter option has obvious advantages, keeping dark counts and crosstalk and more important the gain constant by simply regulating the surface temperature.
Taking into account equation **??**, it appears that the breakdown-voltage can be estimated from the zero-crossing of a linear extrapolation of the gain at every bias-voltage per temperature. By doing this a linear breakdown-voltage dependence of the temperature can be observed. Ap-

pendix Figure(**??**)
I note that the gain, when parametrized over over-voltage, is essentially temperature independent, as I will show later in chapter **??**: Figures (**??**) , (**??**) , (**??**) , (**??**)

2.2 Thermally induced dark counts

Still temp dependent when plotted vs overvoltage Inside the Silicon Photomultipliers depleted region a dark pulse originates from thermal excitation of an electron to the conduction band. Without an event photon present to trigger the avalanche, it is still indistinguishable from a photoelectron pulse. These thermally generated carriers are observed along with with the signal from a real photoelectron, presenting an irreducable source of noise. The number of dark pulses observed is refered to as dark counts ant the number per second as the dark count rate. For applications that need to operate in an environment with low noise, those dark counts are a concern. In IACT application of Silicon Photomultipliers however, this is only a minor problem, since IACTs operate in a naturally noisy environment. Even though sky darkness is one of the prime criteria of the proposed site selections for CTA, the surrounding Night Sky Background (NSB) at the most darkest side in Namibia will still exceed any random noise in the detector. The pollution of those NSB photons is unavoidable noise and will essentially limit the low energy resolution of the telescope to the NSB rate. As long as any random noise, being dark counts or other, is significantly below the NSB rate, it will not affect the telescopes performance.
Telescope performance simulations of the Schwarzschild-Couder MST of CTA at the site of Namibia showed a rate of $\sim$ 20 - 80 MHz per pixel for one of the older SiPM iterations from Hamamatsu. [**??**] This is purely for NSB photons and pixels with a size of 6x6mm^2, the covered range originates from differences in illumination level of the night sky by galactic- and extragalactic-fields. I note that the DCR, when parametrized over over-voltage, remains temperature dependent, as I will show later in chapter **??**: Figures (**??**) , (**??**) , (**??**) , (**??**)

2.3 Avalanche-induced secondary effects

An avalanche originating from the primary cell can sometimes, either directly or by reflection, propagate outside the cell and trigger an avalanche almost simultaneously in a secondary cell. This will, unless accounted for, degrade the Silicon Photomultipliers photon counting resolution, since the signal will be a merge of cross-talk cells and real incident cells. The probability for this is referred to as the cross-talk probability and the effect as the Optical Cross Talk, since it is conveyed via secondary photons generated in the primary avalanche. Afterpulsing also falls under this category, with the main difference to cross-talk being that the carrier triggers a secondary avalanche in the primary cell, basically generating a parasitic pulse inside the previously fired cell. Contained in a single cell, afterpulsing increases the measured charge registered for an incident photon. The difference in arival time of the secondary avalanche distinguishes different

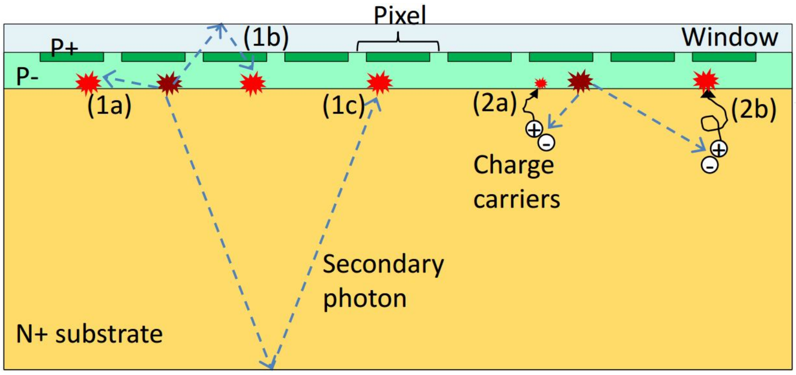

Figure 6: Secondary effects (bright red) caused by primary avalanches (dark red) in a Silicon Photomultiplier. In this paper a single pixel, in this figure, is referred to as a cell (see ??). Everything label under 1 is associated with prompt cross-talk, afterpulsing labeled as 2a, and delayed cross-talk labeled as 2b. Image adapted from [ref]

components comprising the cross-talk and afterpulsing. Those secondary avalanches can again emit photons, that can trigger secondary avalanches themselves, leading to high amplitudes, even in dark conditions.

Figure (**??**) shows different physical processes causing secondary effects in Silicon Photomultipliers based on their delay time. Cause of the delay time is the dependence on the penetration depth of the incident photon, or the region the dark count generated, and the diffusion time inside the substrate. At long delay times afterpulsing and cross-talk are not distinguishable. The prompt Optical Cross Talk happens basically simultaneous to the primary avalanche, since it is unaffected by the primary cells recovery time and is labeled 1 in Figure (**??**). It is either triggered by the secondary photon directly (1a) reaching the neighboring cell, or after first reflecting on the surface layer (1b) or the bottom surface (1c). If the cross-talk avalanche delay time is shorter than the detection resolution, the difference in signal between an Optical Cross Talk event or an incitend photon being detected, is not observable.

Time delayed Optical Cross Talk is caused by a carrier generated in the non-depleted substrate diffusing to a neighboring cell and triggering an avalanche in the depleted region (2b). If the carrier stays in the primary cell, the triggered avalanche is labeled afterpulsing (2a) and will have a lower amplitude, due to the cell not being recovered yet. The delay time is influenced by how deep the carriers are being trapped in the substrate, the time they need to diffuse to the surface, and also distinguished by traps with different lifetimes.

This is very important in IACT performance, since this effect gives random NSB and dark count photons the ability to rise to arbitrarily large amplitudes. The consequent need to raise the trigger threshold to counteract the resulting rising accidental-triggerate has a negative impact on the low energy resolution of the telescope.

Parametrisized with over-voltage, the secondary avalanche effects are temperature independent, shown in chapter **??**: Figures (**??**) , (**??**) , (**??**) , (**??**)

2.4 OCT dependency on cellsize

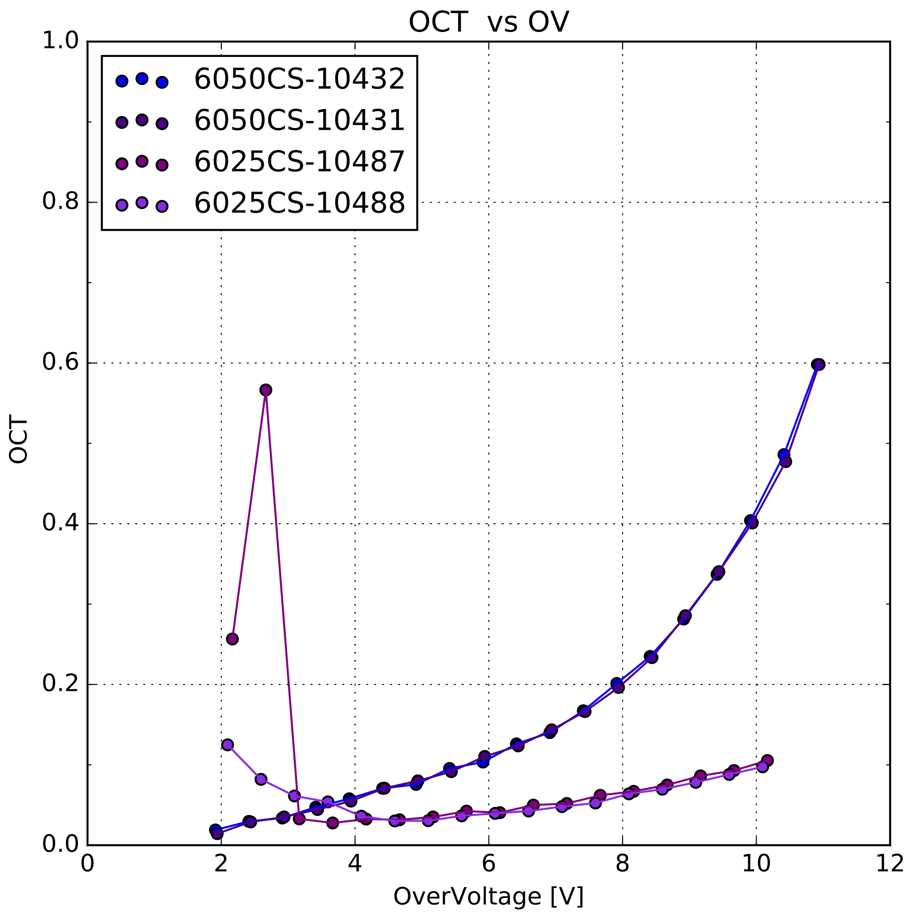

Figure 7: Results of the Optical Cross Talk of 2 sets of 2 similar HPK S13360 devices, that only differ in their respective cell-size. HPK S13360 is the first device incorporating physical trenches in the upper layer, optically isolating each cell. Consequence to this is a drastic reduction in prompt cross-talk. Delayed cross-talk and afterpulsing are basically unafected. Upscaling the 25μm results shows an overlap between the 2, see text.

Cross-talk is dependent on the ability of the secondary photons to reach a neighboring cell. This means, that an increase in cell-size and therefore cell-area should directly correlate with the Optical Cross Talk of a pixel. In Figure (**??** the results of the complete Optical Cross Talk of 2 sets of 50μm and 25μ HPK S13360 devices are shown. Plotting the results of 2 similar devices, only different in their cell-size, and then multiplying the 25μm results by the factor derived from their difference in area, here 4, a correlation is visible. Scaling up the Optical Cross Talk of the 25μm cell, shows an overlap between the 2 cell-sized pixels. This means, that the Optical Cross Talk is directly area and therefore cell-size dependent.

Since the measurements conducted by me do not differ between the range of secondary avalanche effects, the Optical Cross Talk shown contains every aspect.

2.5 Photon Detection Efficiency

The Photon Detection Efficiency is the probability of a detector to absorb an incoming photon and produce a measurable signal at its output, and depends on a number of factors. First the photon must enter the depleted region via transmission through the surface of bare silicon, which has a reflectivity of 30%. However, the transmission probability can be improved by coating the surface with a substrate with adequate thickness and a refraction index between air $\eta_{air} = 1.$ and silicon $\eta_{silicon} = 3.4$. Devices presented in this paper are coated with epoxy, a silicon resin and glass. The coating also has the added benefit of insulating and protecting the cells against environmental influence. A possible negative effect of coating is an increase in prompt cross-talk and a larger dependency of the overall cross-talk on the cellsize. The second factor is quantum efficiency, describing how susceptible the depleted region is to photons exciting electrons from the valence band to the conduction band. This is sometimes refered to as spectral response of a detector to reflect the wavelength dependence of a detector and makes the PDE wavelength dependent. The over-voltage dependency of the PDE is conveyed by the third factor, the avalanche probability. It depends on the electric field present, and thus on the applied over-voltage. The last factor is the fill-factor: the more the surface area of the detector is covered with active-area cells and the less dead-area exists between cells the higher the fill-factor is.
The Photon Detection Efficiency is commonly measured by illumination of the pixel and a calibrated reference photodiode with a flashing light source, and determining the average number of photons hitting the photosensor during a light pulse.

$$PDE = \frac{N_{detected\ photons}}{N_{total\ photons}} \tag{3}$$

Figure 8: Photon Detection Efficiency is the percentage of detected photons versus overall emitted photons.

3 Imaging Atmoshperic Cherenkov Telescopes

3.1 Cherenkov Radiation

Because our atmosphere is opaque for gamma radiation, gamma ray astronomy was mainly done by satellite based instruments like FermiLAT. That said, we can still see their effects on earth, in the case a gamma ray hits an air atom in the atmoshpere, getting scattered and creating a particle shower. In this air shower, the initial and each subsequent particle emitt Cherenkov light. Cherenkov radiation is a phenomenon caused by charged particles traveling faster than the local speed of light would allow in that medium. This light is emitted in a narrow cone with an increasing angle as the particles travel downward. This Cherenkov light shows as a very short ($\sim$5ns) flash with a peak in the UV-spectrum at around 330nm. Thus, we can image the particle cascade measured with the telescope and can reconstruct their path. We can use this stereoscopic view of the shower to reconstruct where our source of gamma rays is in the sky.

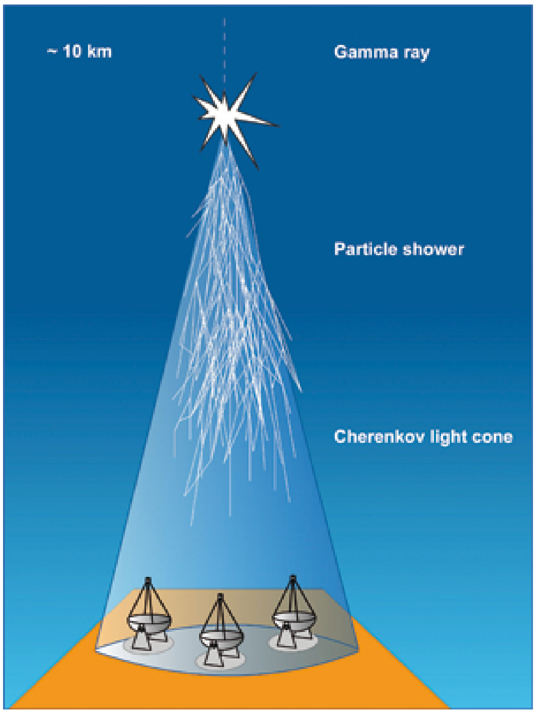

Figure 9: The cone of Cherenkov light emitted by an extensive air shower

Is is also possible to reconstruct the energy of the original photon from the amount of light produced. This is possible because energy is conserved, so all energy of the original photon is now distributed between the particles of the shower.

Sources include our galactic center, Supernova remnants, Pulsar Wind nebulae, but also extragalactic sources like active galactic nuclei or gamma ray bursts.

That is, if the original particle was indeed a gamma photon. There are other charged high energy particles we could also detect, namely atomic nuclei or electrons, which could collide with the atmosphere producing similar events. So, to determine whether it is a hadronic or gamma shower we look at many different shower characteristics like diffusion , compactness, and the ratio of width and length.

Before, gamma ray astronomy was mainly done using satelite based instruments. The technique behind the ground based experiments called Imaging Atmospheric Cherenkov Telescopes

(IACTs) aims at measuring the time, direction and energy of flashes of Cherenkov light from extensive air showers caused by high-energy gamma radiation. The range of the Cherenkov flash being between 300-600nm, current generation SiPMS are a promising candidate to replace the progenitor photon detector used in previous experiments like HESS, the Photomultiplier Tube (PMT).
Current ground based IACTs consisted of mostly 4 telescopes, HESS, MAGIC, Veritas among them.
All of those arrays consist of at most 5 telescopes spread over a wide area. So most cascades are viewed by only 2 or 3 of the telescopes.

3.2 Cherencov Telescope Array

CTA stands for Cherenkov Telescoipe Array and is an advanced ground-based observatory array of many tens of telescopes distributed over a larger energy range than before. It will allow detection of gamma rays over a large area on the ground and from multiple different directions. We can use this stereoscopic view of the shower to reconstruct where our source of gamma rays is in the sky. The array will consist of 60 - 100 telescopes of different designs and sizes to cover the aimed for energy range and area. There are currently 2 sites planed.

1. A southern cta site, with an array consisting of three types of telescopes:

   a) LST The low energy instruments, between 20 and 200 GeV, will consist of four 23 meter class telescopes with a moderate field of view (FoV) of the order of about 4.5 degrees.
   b) MST The medium energy range, from around 100 GeV to 10 TeV, will be covered by 24 telescopes of the 12 meter class with a FoV of 7 degrees.
   c) SST The high energy instruments, operating between a few TeV to 300 TeV, will consist of about 72 small (4 meter diameter) telescopes with a FoV ranging from 9.1 to 9.6 degrees.
   d) footnotes
   e) (area covered by the array of telescopes: 4 km^2)

2. CTA Northern Site:
   a) 4 large-size telescopes and 15 medium-size telescopes
   b) (area covered by the array of telescopes: 0.4 km^2)

There are currently 3 different prototypes in development for the SST variant: SST2M Astri and GCT , and a siglee mirror prototype SST1M

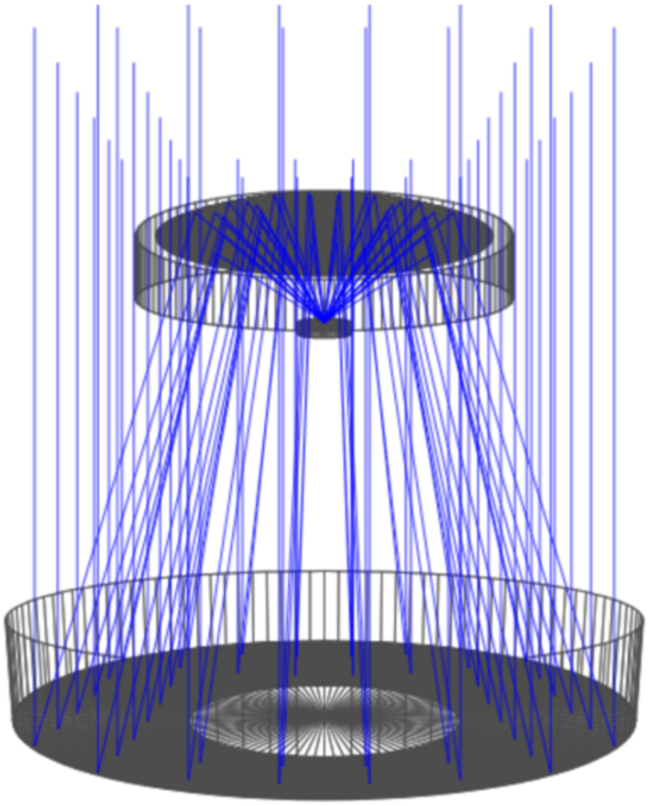

Figure 10: Schwarzschild-Couder Optics, If possible replace picture with GCT with mounted CHEC camera picture here

This papers work is conducted on the GCT design, one of the prototypes for the high energy telescope called SST-2M GCT utilizing a 2 mirror design called Schwarzschild-Couder.

3.3 GCT

The 2 mirror design of the telescope allows us to utilize SiPMs. Current IACTs have a parabolic optical system, which is reliable and efficient but they need to be large in order to have a large FoV due to aberrations, resulting in huge CAMERA plate scales and therefore expensive assembly of photodetectors.

Schwarzschild-Couder have no such aberrations, at least not on our scale, while the IACTs can still have a very large f.o.v. up to 15° without significant degradation of the spot size. The resulting physical pixel size is more compact than that of the single mirror optics and cost-effective photon sensors such as multi-anode photomultipliertubes (MAPMTs) (like in CHEC-M) or Silicon Photomultipliers (SiPMs) can be used for the camera.
There are of course disadvantages, the optical system will be more complex, with tighter tolerances.

In summary it reduces the camera plate scale, allowing us to use SiPM photosensors.

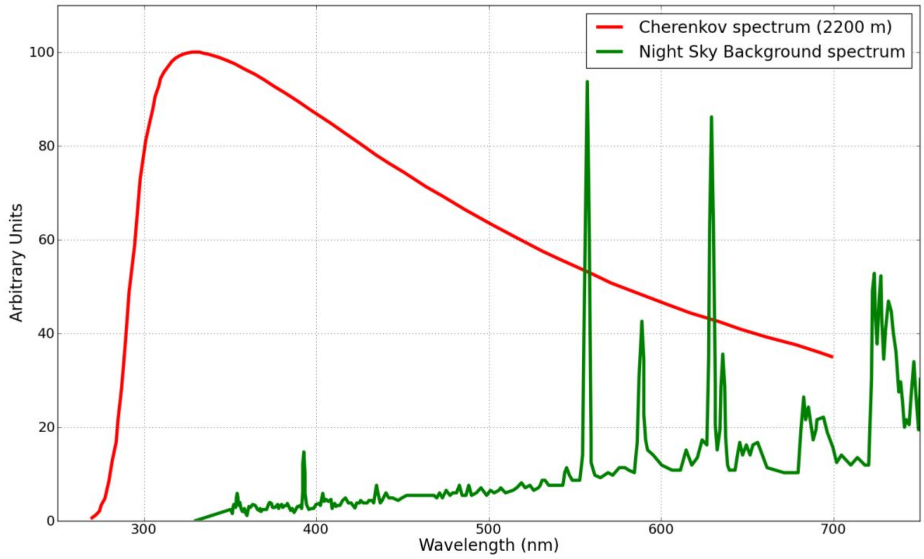

Figure 11: The spectrum of Cherenkov light observed from an extenden air shower at 2200m asl. compared to the expected NSB measured in La Palma. Units on the y-axis are arbitrary because NSB and Cherenkov light vary by different parameters. Image from [??]

3.4 CHEC-S

CHEC-S Target Modules (with pic)

3.5 SiPM requirements for CTA

In order to make an educated choice on the best SiPM device to use to populate the cameras focal plane, an in-depth characteristic study on pulse-shape, gain, temperature-dependence, detection efficiency, thermal noise and correlated secondary effects is conducted by multiple groups within the CTA collaboration.
This paper studies noise from thermal, as well as secondary effects and their temperature dependence. To be considered a promising candidate, any given SiPM device must have a high enough fill-factor to guarantee high PDE. This is necessary to ensure the something about data loss in CTA requirements? . The peak of the spectral response of the SiPM is desired to be around the spectral peak of the Cherenkov light and at the same time, must have a fast enough drop to ensure less NSB pick up (Figure(**??**)). The overall noise from thermal and correlated secondary effects of the SiPM must be sufficiently below the expected NSB rate at the location (usually around ∼20-80 MHz). Additional?

4 Experimental Setup

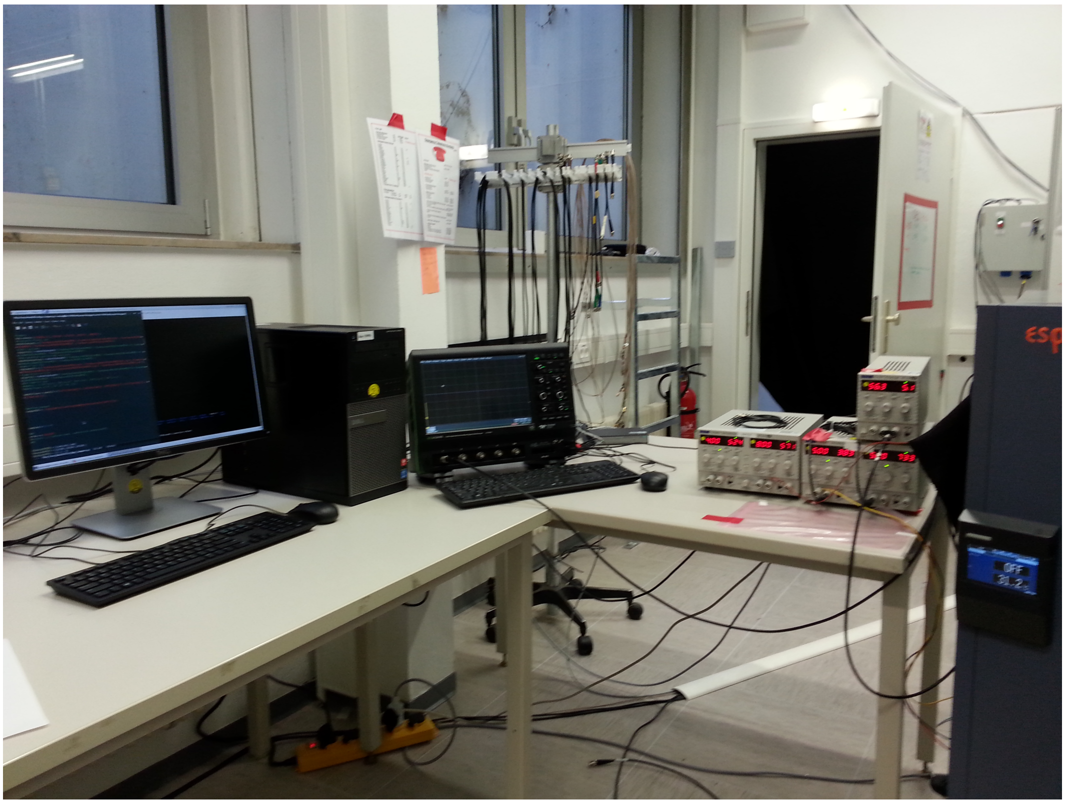

Figure 12: Will be updated. With Alphabetical captions for the different steps and references later in the text and setup scheme below, Picture of the inside of the thermal chamber is missing, will do later, and try to fit it next to this one

The experimental setup in general is designed to house a variety of SiPM devices. Over the course of this paper, 5 different types of SiPMs were mounted on the setup and evaluated. It involves a thermal chamber Figure(**??**)(A) for temperature regulation which proved light tight and thus also serves as a dark box, to prevent any stray light to reach the SiPMs surface. Depending if the SiPM Figure(**??**)(A1) in testing is pre-manufactured on a test-array or supplied as a standalone chip, it is either mounted directly on a mechanical arm inside the chamber in the former case, or in the latter the mechanical arm supports a specifically designed PCB connecting to the device. Via the mount, bias-voltage is supplied and signal is transfered to the shaper Figure(**??**)(A2). !!!!!Need some more details on shaper

In some cases the output signals amplitude is to low to trigger the oscilloscope, therefore amplification is needed. I used an amplifier from MiniCircuits ZFL-1000-LN+ SN:283401542 Figure(**??**)(A3) supplied with different voltages depending on the tested device to amplify the shaped signal.

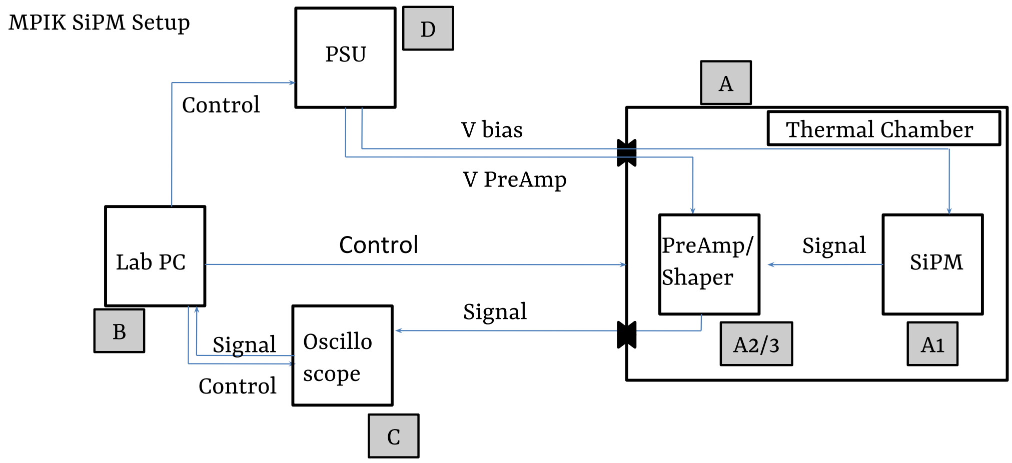

Figure 13: Experimental setup scheme

Data acquisition in the Laboratory is realized by a Lab-PC Figure(**??**)(B) , that forms the central control station for multiple pieces of equipment. It is connected to the oscilloscope Figure(**??**)(C), which records the waveforms of the device in testing, and then sends the data back to the PC via ethernet. The oscilloscope is a Lecroy XXXXX SN capable of 2.5 $\frac{GS}{s}$. The power supplies Figure(**??**)(D) control the bias-voltage of the Silicon Photomultipliers, ramping of the bias-voltage is controled by the PC. Lastly the thermal chamber is connected to the Lab-PC, which controls the temperature, and continuously rechecks it during temperature ramps. Signal transfer from the shaper to the oscilloscope is via a throughput on the side. All equipment is connected via ethernet, plugged into a common hub, to form a local network. While the temperature of the thermal chamber is ramping from the previous to the next set-point, the data is send to the Lab-PC.

Temperature regulation is an issue in the teststand, as there is no way of controling the SiPMs surface temperature. In dark conditions however, without conducting illumination tests, the shift in temperature on the SiPMs surface is only minimal. (Find the breakdown-voltage dependence on temperature in the appendix (**??**). Checking the surface temperature of all devices with a temperature probe during testing showed minimal rising temperatures. So the influence of the temperature on the breakdown-voltage is only of minor concern. However, once illumination tests begin, the rising temperature on the SiPMs surface will no longer be negligible and the temperature must be regulated, either by cooling of the surface or including the temparature parameter.

5 Data Analysis

The analysis of the Silicon Photomultiplier waveforms is done exclusively in python following the sequence:

1. data conversion
2. pedestal subtraction
3. peak detection
4. gain extraction
5. calculation

The waveform data, after being transfered to a seperate PC, is analyzed offline. The goal is to extract event-data from the waveforms in order to produce pulse-area spectra for every bias-voltage at every temperature. To that end, the pedestal of the electronic noise must be found and subtracted from the data. After that, event-pulses are detected and integrated. This generates a list of pulse-areas, which is in turn used to fill a pulse-area histogram. To this pulse-area histogram, a model is fitted from which the gain can be extracted. Due to the linear behavior of the gain with rising bias-voltage, a regression line is fitted, from which the Dark Count Rate and the Optical Cross Talk are calculated using the original pulse-area histogram.

5.1 Tracefile Conversion

The oscilloscope produces the waveform data in its intrinsic data format, called a trace with the data suffix trc in binary. A trace file contains a header and two binary lists, an amplitude based on the oscilloscopes voltage-range and offset, and a list of the same length containing the associated event-time, based on the time-range and horizontal offset. The first step is therefore a conversion of the amplitude and associated event-time of all segments of a waveform trace file into two lists of floats.

5.2 Pedestal Subtraction

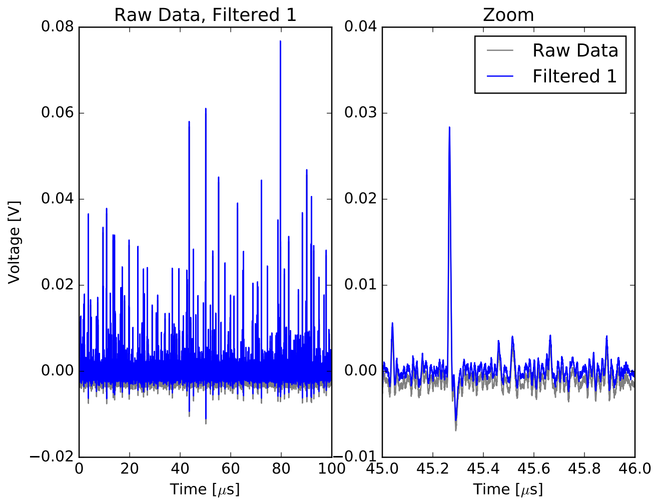

Figure 14: Pedestal subtraction++

A single waveform from the oscilloscope is anticipated to be uncentered, it will be slightly above or below zero, depending on the device setup (some devices produce inverted signals). The signal is mixed with electronic noise when it is observed and forms a pedestal, shifting the mean of the waveform from its original position to zero. Pedestal subtraction removes this average noise.

The first step of the process is reading in the uncentered waveform and calculating an initial mean(mean0), expected to be slightly higher than the actual mean of the noise, due to the presence of event-pulses. The waveform is then shifted to about zero, by subtracting the mean0. A second mean of the now nearly centered waveform is taken (mean1). Now a new, same-sized array is formed and filled with the data from the waveform that is smaller than mean1, this represents the negative noise. The data larger than mean1, the positive noise, is also filled into the array, but is negative-signed. This creates an array of the waveform centered around zero and, above the mean1, folded towards the negative. It proved reliably, that calculating the root-mean-square of this helper-array is a solid possibility of stripping the waveform of event-peaks. Taking the root-mean-square with a factor 3 of the helper-array, a cut is now applied to the waveformon on both, the positive and negative side. In that fashion, the remnant is the waveform between the positive and the negative root-mean-square and is now called a peakless-signal, representing the noise of the waveform.

Pedestal subtraction is done by calculating the mean of this peakless signal and subtracting it from the waveform. After that, the peakless signal is also smoothed by convolving it with a wide-windowed gaussian and subtracted from the waveform to eliminate any slow moving noise.

5.3 Peak Detection

Peak detection exploits the fact, that the first derivative of an event-peak will cross zero into the negative at the peak maximum. The presence of random noise in the signal however will lead to many false detections. Therefore, before the detection of the event-peaks, the waveform is smoothed with a narrow-window gaussian with a width of about the FWHM of the devices characteristic event-pulse, in order to attenuate non-event peaks. After the first derivative of the signal is calculated, which in python is a fast process if using arrays, a number of parameters decide the validity of the detected peaks. Most important parameters are a certain predetermined minimum amplitude, called the amplitude threshold or: minimum peak height. This is right now determined by eye, but could later be calculated based on the noise level. The second important parameter defining validity is the minimum peak distance, which defines how close two events can occur after another. The value is determined by the FWHM of the device in testing, which I expect to be sensible enough to resolve two events happening close after another. The peak detection algorithm can not distinguish between instantanious and delayed Oprical Cross Talk, but nonetheless, due to the fact, that the signal data is taken over many micro-seconds, all events are detected, independent of their source. On the other hand, this also means, that it is possible for two events to happen at the same time, for example a real photoelectron-event coinciding with delayed Optical Cross Talk. This can not be destinguished and will lead to a slight shift of the amplitude. (because delOCT is partial 1p.e.)

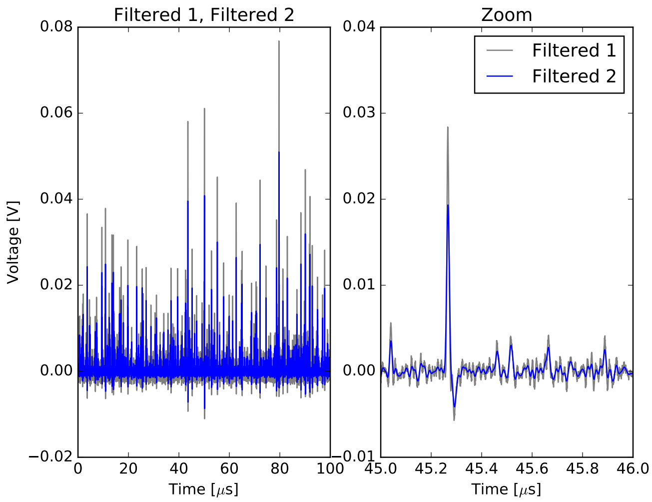

Figure 15: Peak Detection

The detected peaks are integrated with a window extending symmetricaly from the peak maximum, the width is chosen as slightly wider than the peaks FWHM. The generated list of peak areas is generating a peak area histogram, which is fitted with multiple gaussians using iMinuit in python , seen in Figure (**??**). Two parameters are extracted from the fit to the peak area histogram. The first, the position of the 1p.e. peak is the position of the maximum of the first peak in the histogram, and the position of corresponding multiple p.e. events should be integral factors of the 1p.e. position. This proved to not be the case for some devices, the suspected source of this error is a pedestal generated during the peak integration. I studied the effect of the integration window in more detail in chapter **??**. A second parameter is extracted from the peak area histogram to deal with this problem, which is the distance between N p.e. peak maxima of the histogram, labeled Δp.e. , which defines the gain. The apparent pedestal of the pulse area histogram makes extraction of the two parameters necessary in order to calculate the Dark Count Rate and the Optical Cross Talk.

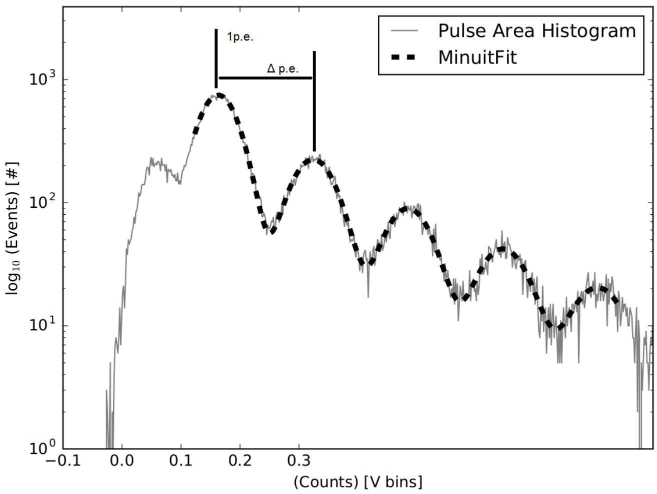

Figure 16: Pulse Area Histogram todo describe more

The gain of a Silicon Photomultiplier has a linear dependence of the supplied bias-voltage. Given that the bias-voltage range is deliberately chosen such that the over-voltage ranges from about 1V growing upwards, the range of linearity only starts at around the point of operation given by the manufacturer of the device. At the higher end of the bias-voltage range the behaviour usually starts to divert from the linearity. In order to get an estimation of the gain over a large range, both previoulsy extracted parameters, the 1p.e. peak and the distance Δp.e. are fitted with a linear regression line. The fit assumes linearity utilizing weighted least

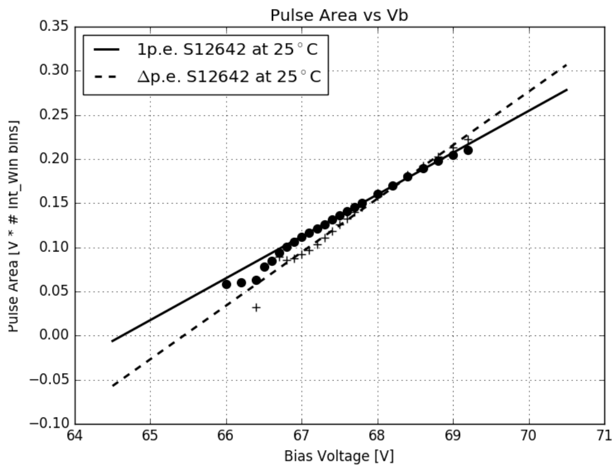

Figure 17: 1p.e. position and Δp.e. plotted versus bias-voltage

squares inherited from pythons statsmodels package. Fot the fit, only the data, where at least 3 gaussians are fitted to the peak area histogram is taken into account. Plotting both extracted parameters, as well as their respective regression lines versus bias-voltage, as in Figure (**??**), shows the difference between the two parameters. (SHOW FOR ALL DEVICES IN APPENDIX???). Comparing the manufacturer supplied brakdown-voltage from the datasheet for all devices showed, that the zero-crossing of the 1p.e. regression line is more consistent with datasheet values, in contrast to the zero-crossing of Δp.e. , which lies slightly higher. The over-voltage, corresponding to the set bias-voltage at any given temperature is calculated from this breakdown-voltage. Dark Count Rate and Optical Cross Talk are calculated utilizing 1p.e. position and Δp.e. derived from the regression line. Both values are applied, in the calculation, to the peak area histogramm with the Dark Count Rate being defined as:

$$DCR = \frac{N_{events(>0.5p.e.)}}{T_{experiment}} \tag{4}$$

Figure 18: The Dark Count Rate of a Silicon Photomultiplier is defined as all events exceding 0.5 p.e. in apmlitude $N_{events(>0.5p.e.)}$ occuring over the experiment time $T_{experiment}$. Included in the measurement are thermally generated dark counts, as well as delayed cross-talk and afterpulsing with only a minor contribution.

,and the Optical Cross Talk as:

$$OCT = \frac{N_{events(>1.5p.e.)}}{N_{events(>0.5p.e.)}}. \tag{5}$$

Figure 19: The Optical Cross Talk of a Silicon Photomultiplier is defined as all events exceding 1.5 p.e. in apmlitude$[N_{events(>1.5p.e.)}]$ devided by all events exceding 0.5 p.e. in apmlitude$[N_{events(>0.5p.e.)}]$. It scales with the number of photons produced inside an avalanche, as well as the probability of these photons to trigger a neighboring cell

5.5 Data Challenges

5.5.1 The influence of the minimum peak distance

The influence of the minimum peak distance is shown in Figure (**??**) . Based on their bin-width, four different windows are tested. With the oscilloscopes sampling rate of $2.5\frac{GS}{s}$, the windows of 100, 63, 25 and 13 time-bins, correspond to 40, 25, 10, 5 ns windows respectively. With a

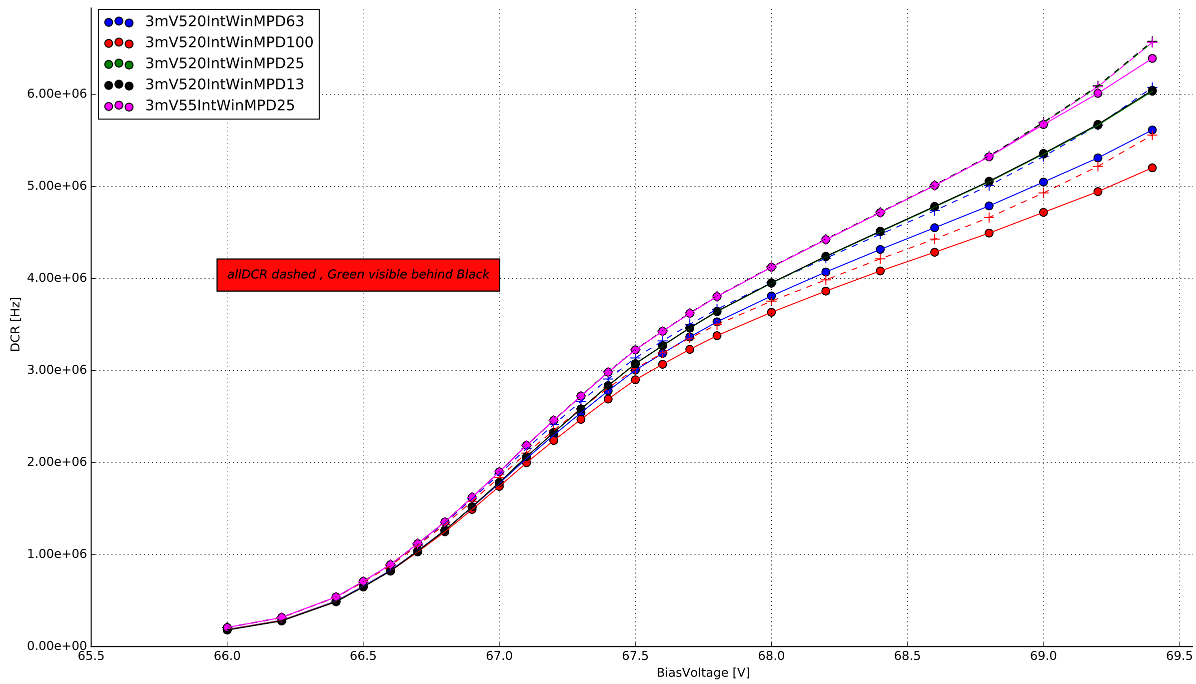

Figure 20: The difference between 4 minimum peak distance windows, in time-bins, during the peak detection. The dashed lines are the Dark Count Rates considering all recorded events, forming an upper limit. In pink, the effect of a different integration window is shown.

event pulse FWHM of 10ns, setting the minimum peak distance to 100 bins, resulting in a 40ns window is visibly to large, as the algorithm will skip over valid data Figure (**??**)(red). After an event is detected, skipping over 40ns worth of data will result in errors of the Dark Count Rate, since the calculation uses the complete experiment time. Therefore a more reliable distance window must be chosen. The second window of 25ns was the next approach, originating from the length of the pulse-tail Figure (**??**)(blue). This would lead to no detected events overlapping with the tail of one previouly detected, resulting in a sharper pulse-area spectrum. Compared to a window of approximately the pulse FWHM, the previously discussed window would still lead to lost event-data. Since the sharpness of the pulse-area spectrum is already sufficient, a window around the pulse FWHM was chosen as reference for all measured devices Figure (**??**)(green). Going lower that the pulse FWHM showed no improvement Figure (**??**)(black).

5.5.2 The influence of the integration window

Figure (**??**) also shows the influence of the size and shape of the integration window on the Dark Count Rate. The influence of the chosen integration window is most visible in their respective pulse area spectra. Choosing a narrow, symmetrical integration window of 5ns left and right of the peak maxima, the noise peak, or zero-peak, is much more prominent compared to the pulse area spectrum of a symmetrical 10 ns window. This leads to errors in the multi-gaus fitting step, or the fitting will fail alltogether. An asymmetrical integration window of 5ns left, 20ns right, to capture the influence of the pulse-tail proved, at first, to be the best solution as their was no visible zero-peak present. The low amplitude pulses are averaged out by the extended integration window to the right of the pulse-maximum. The downside of the asymmetrical window is the shifting of the puslse area spectrum and the fact, that the N p.e. peaks get blurred. The next step was widening the window on both sides. This proved the best solution, since there is no zero-peak visible and the N p.e. peaks are gaussian shaped. Please see the Appendix for the respective plots of pulse area spectra of the different windows **??**.

5.5.3 The influence of the peak detection threshold??

Choosing an adequate peak-finding threshold is a crucial step. Compared to a threshold of ∼0.5 p.e., setting the threshold low will cause the peak finding algorithm to misinterpret a lot of noise peaks as actual dark incidents. This, of course, leads to errors in the gain extraction and even if a gain regression line can be extracted, the resulting Dark Count Rates and Optical Cross Talk will be incorrect. Figure (**??**), shows the effect a low peak finding threshold has on the Dark Count Rate.

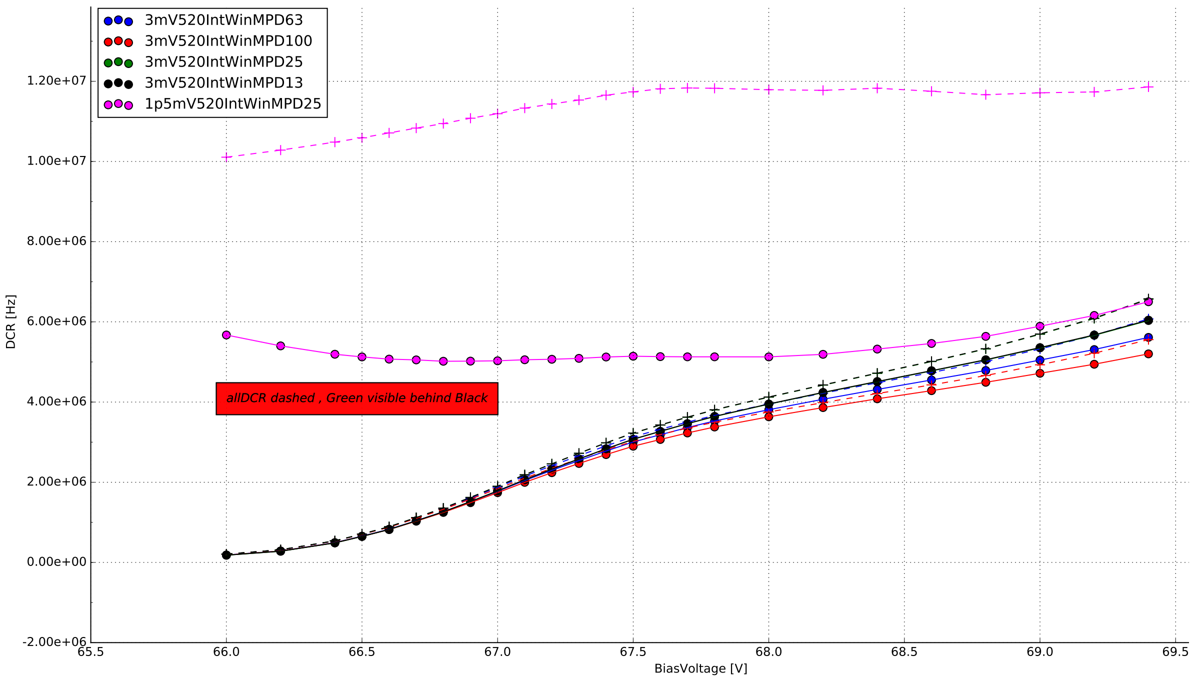

Figure 21: The difference between 4 minimum peak distance windows, in time-bins, during the peak detection. The dashed lines are the Dark Count Rates considering all recorded events, forming an upper limit. In pink, the effect of a lowered peak detection threshold is shown.

6 Results

6.1 SiPM devices for CTA

Manufacturer	pixel size	cell size	coating	connection	specifics	pre-Amp
HPK S12642-1616PA-50 *CHEC-S SiPM	$3mm^2$	50μm	SR	TSV	no trenches	CHEC-S buffer
HPK LCT5 S13360-6050CS	$6mm^2$	50μm	SR	wire-bonds	trenches	MS 13V
HPK LCT5 XXXXXXXXX	$6.915mm^2$	75μm	SR	wire-bonds	trenches	MS 8V
HPK 6050HWB-LVR-LCT	$6mm^2$	50μm	SR	TSV	trenches	MS 13V
SensL FJ60035	$6mm^2$	35μm	glass	TSV	no trenches	MS 15V

Figure 22: List of SiPM devices which results are presented in this paper. *(SR: silicon resin , MS: MiniCircuits , TSV: through silicon via)

Silicon Photomultiplier devices for CTA are researched by many different groups, validating different characteristics. Besides the current SiPM for CHEC-S, newly developed prototypes offer a diverse range of pixel- and cellsizes. The majority of the devices are tested in Japan, at the University of Nagoya, conducting in depth analysis of the characteristics over a wide overvoltage range at one static temperature, mainly focusing on PDE and OCT, and their correlation. This correlation of OCT and PDE for all devices determines the candidate for CHEC-S, by comparing the highest PDE at the lowest possible OCT for each device. At MPIK, chosen candidate devices are examined regarding their temperature dependence and as to assist in the final decision by confirming results with a different analysis technique.
The chosen devices include the current CHEC-S device HPK S12642-1616PA-50, from Hamamatsu Photonics K.K., to be implemented in the first prototype camera. It is a previous generation SiPM, which was decided for use in 2014.(, due to the limited availability in high PDE devices at that time.) The manufacturer supplies a 16*16 channel premounted tile of 3mm^2 pixels with a cell-size of 50μm. To emulate the usage in a TARGET module, 4 3mm^2 pixels are electrically connected to form a 6mm^2 superpixel. The tile is typically coated with epoxy resin, but due to specific requirements regarding the uniformity of the coating, it was replaced with a very thin layer of silicon resin equivalent to later prototypes. The CHEC-S devices electronical connection is realised via the new through-silicon-via (TSV) concept of running a connecting solder through the silicon bulk, instead of wiring on the outside, greatly increasing the fill-factor, but also including some disadvatageous sideffects later shown.

Additional tested devices include the LCT5 generation from Hamamatsu Photonics K.K., so called due to their low cross talk properties, namely the commercial available S13360-5050CS. This device is the first to include physical trenches between the cells, effectively dividing the cells optically and thus reducing prompt cross-talk probability.
The LCT5 generation also made two prototype devices avaiable for testing at MPIK, the first, HPK LCT5 SN CATANIA, is a larger iteration with a cellsize of 75μm and a pixelsize of 6.915mm^2. Being from the LCT5 generation it also includes optical trenches. The second device available is a LCT5 prototype designated 6050HWB-LVR-LCT , LVR meaning low-voltage-range, with the same physical dimensions and properties as the S13360 device but incorporating TSV technology and possibly other unknown deviations.
The final device is a commercially avaiable test-array designated FJ60035 from SensL, pre-mounted on a test-array by the manufacturer. It has the same pixel-size, but a much smaller cell-size 35μm than the previous mentioned devices and a different coating (glass).

The tests conducted in Nagoya contain many different iterations of the LCT5 generation with variing pixel- and cell-sizes.
For a full overview of the considered Silicon Photomultipliers, please refer to the appendix under (**??**).

6.2 Hamamatsu S12642-1616PA-50 50μm 3mm

The Silicon Photomultiplier by Hamamatsu Photonics designated S12642-1616PA-50 is a 3 mm by 3 mm device. The array uses the through-silicon-via technology, meaning there are no wire-bonds present, the electrical connection is realised through the silicon-body. The pixels are coated with a thin film of silicon resin, after the previously used epoxy resin proved not uniform enough. One array consists of 256 pixels, 4 of which are electrically tied togother to form a 6mm by 6mm superpixel respectively. This practice is necessary for the pre-production camera CHEC-S, because the focal plane is mechanically designed to house 64 6mm^2 pixels, connected to the TARGET modules. Furthermore I expect this to have an influence on my results due to electrical crosstalk, but this is only of minor concern due to the following. My measurements of the CHEC-S tile concentrate on the array as an as-is device. This means all results, influenced by external factors outside the actual Silicon Photomultipliers physics, are valid on the assumption, that the way I was conducting the measurements is the way the Photomultiplier will later be incorporated into the camera. On that ground, deviations of my results from the results of other groups and the manufacturer itself are expected. To clarify this further, I expect, for example, that the tests done at Hamamatsu Photonics where conducted on a single 3mm^2 pixel, not an array of 256 pixels, where 4 are tied together. Also divergence of shaping and amplification electronics between the groups will result in some differences. For this test, the CHEC-S tile is connected to the CHEC-S buffer, supplied with ±4V, where the signal is amplified. This signal in turn is then shaped via the CHEC-S shaper, developed by the University of Leicester. This is done in order to lower the unshaped pulse from a FWHM in the 100s ns to 10ns. This whole amplification and shaping chain is simulating later usage in the TARGET modules. I conducted the measurements multiple times on different pixels of the CHEC-S tile.

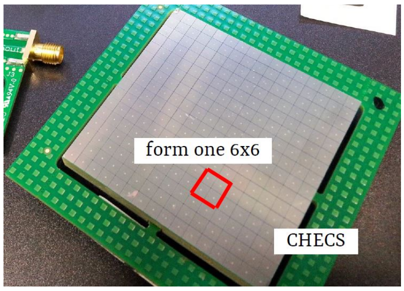

Figure 23: CHEC-S tile

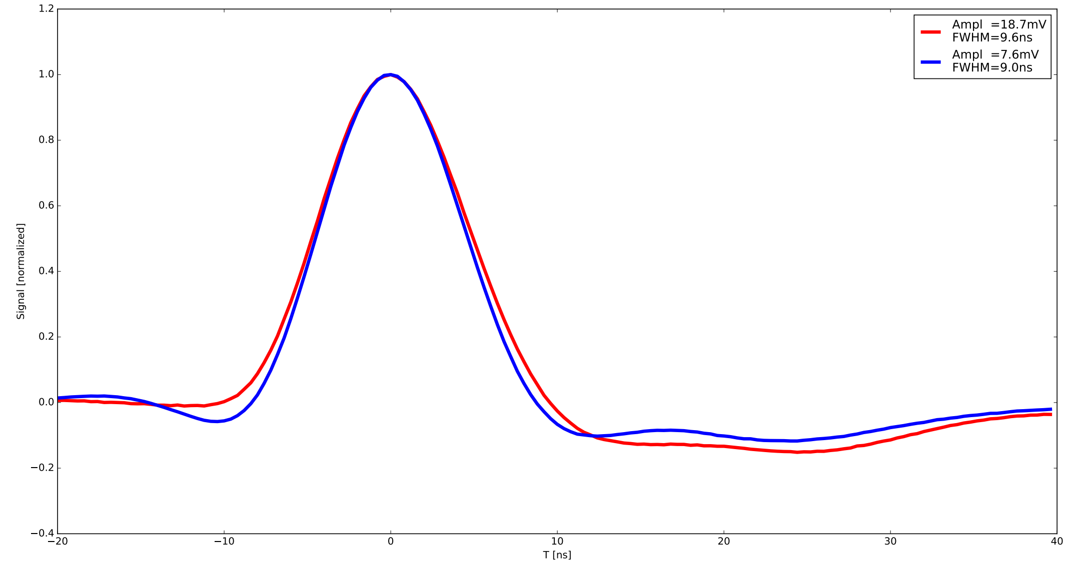

Figure 24: The average pulse shape of the 1photoelectron in blue and the 2photoelectron pulse in red of HPK S12642 at 25° C and 67.8V, which is around the proposed operating point. Both pulses are averaged over »1000 events and normalized to illustrate possible differences in pulseshape resulting from the utilized shaping electronics. Both pulses have a FWHM of around 10ns and are nearly free of ringing. The resulting average amplitude of the 1p.e. pulse is later used to calculate the Gain in [mV/p.e.] instead of [V*IntWin] by cross-referencing the 1p.e. amplitude at multiple bias-voltages.

6.2.1 Gain

As descibed in section**??**, the average pulse shape fig(**??**) is used to convert the relative gain from the analysis procedure to an absolute gain in sensible units. This is necessary, because the analysis aims to use pulse-area rather than -height, which results in this relative gain being in units of $V * timebins$, instead of plain V. In Figure (**??**) (left) the relative gain is shown, the right side shows the gain after conversion. A lower gain with increasing temperature is expected and described in detail in the chapter **??**. In short, increased lattice movement due to higher temperature hinders photoelectron transport. The effects visible at extreme bias-voltages at both ends are partially analysis related. The gain of a SiPM is expected to be linear over bias-voltage at a constant temperature.

In the lower regime at Vb 66.5V my analysis method struggles to pick up pulses, because of the very low gain compared to the noise. Depending on the chosen peak-finding threshold, I expect the analysis to interpret noise peaks as 1p.e. peaks at an increasing rate, the lower the overvoltage is. This is visible in the sudden break in linearity at 30° C and 35° C , where the gain is almost in a plateau, due to this effect. The roll-over of the gain at the highest bias-voltages is in part a result of a voltage drop across the bias resistor occuring, because of high current flow

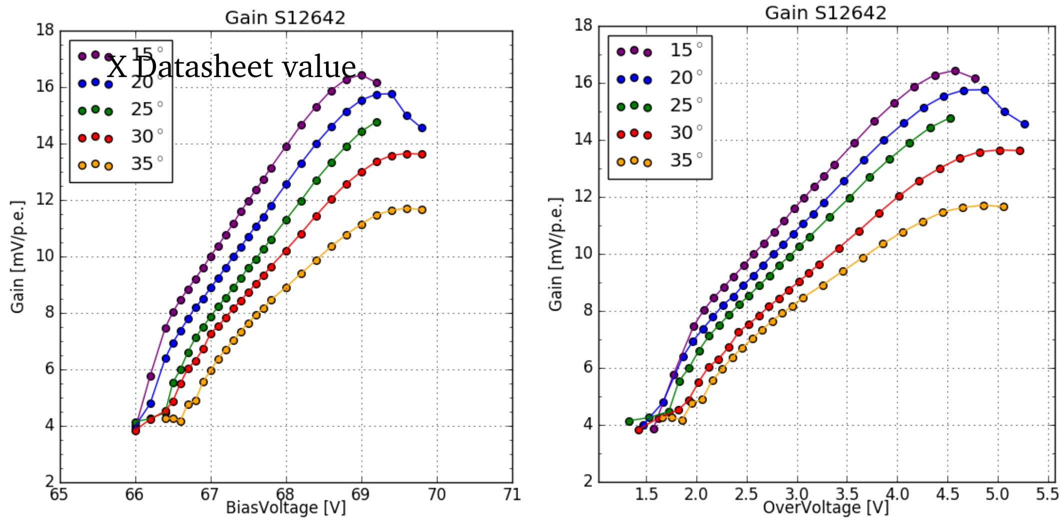

Figure 25: Gain of the HPK S12642 pixel, plotted against over- , bias-voltage and temperature.

through the SiPM. At higher temperatures, and therefore higher dark rates, the effect occurs at lower over-voltages. A second influence is caused again, by the noise at Vov 5V, which is very high compared to the proposed point of operation at Vov 3V. The same threshold is again counting the now increased noise peaks as 1p.e. peaks, but due to the abundance of 1p.e. pulses this just results in an apparent lowering of the gain.

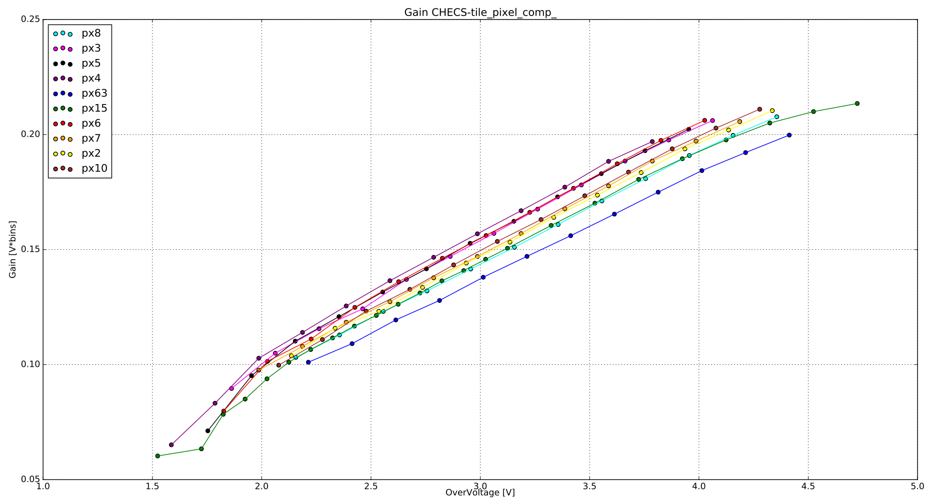

Figure 26:

6.2.2 Dark Count Rate

The Dark Count Rate is expected to increase with temperature, which is the case for S12642 showb in Figure (**??**). I also expect it to follow a nearly linear progression, a sudden turn-up or turn-down of the Dark Count Rate would be analysis related. The turn-up at a certain point is visible in Figure (**??**), particulary for 15° C (purple) and 20° C (blue) respectively. At 15° C and an Overvoltage of 4V, the Dark Count Rate starts to deviate from the previously linear behaviour. It starts to rise more rapid than before, which I can attribute to the fact, that the Optical Cross Talk at that point is very high; higher than 50% fig(**??**) (left). I suspect that I do not reach this critical point for the higher temperatures of 25° C (green) and 30° C (red), so the effect is barely, if not at all visible. At 35° C (yellow) I suspect my analysis is not able to count every

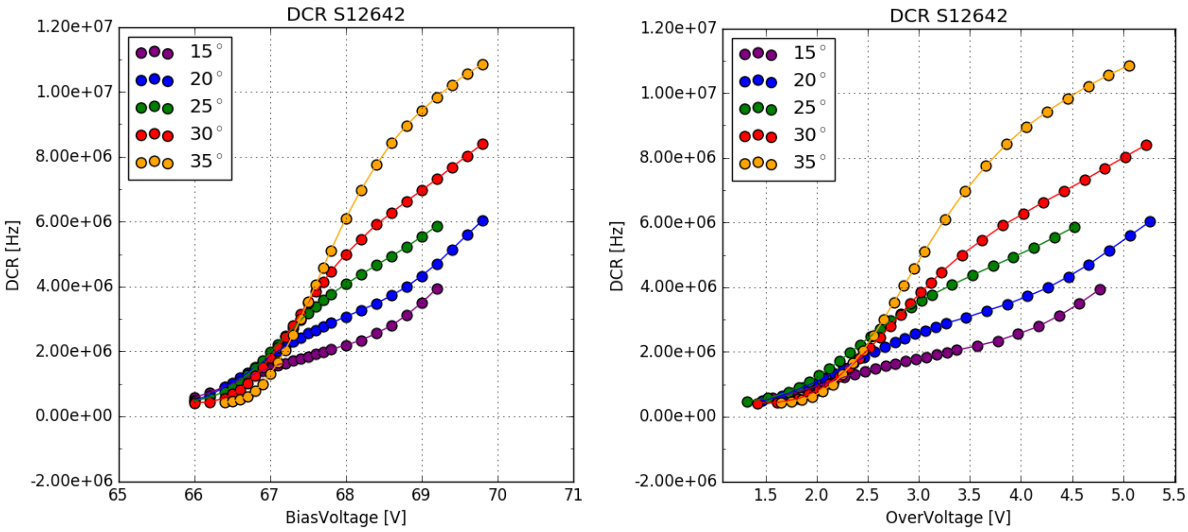

Figure 27: Dark Count Rate of the HPK S12642 pixel, plotted against over- , bias-voltage and temperature.

pulse, due to the high rate of 9-10 MHz. A majority of the pulses overlapping each other and being counted as a 2p.e. event rather than 2 1p.e. events would reduce the Dark Count Rate significantly. At this point, heating of the Silicon Photomultipliers surface due to the high rate could also affect the Dark Count Rate through shifting of the temperature slightly upwards, away from 35° C . So that the Dark Count Rate declared at 35° C is in reality the rate at higher temperatures.

At the lower end of the bias-voltage range, I suspect, that a major part of the found 1p.e. pulses are actually noise related. So the Dark Count Rate changing to a plateau is expected. This is also due to the fact, that my measurements are done with a fixed bias-voltage range. Due to the increase of the breakdown-voltage with rising temperature, part of the measured bias-voltage range corresponding to a very low over-voltage, attributes to this effect. In order to reliably measure beyond an overvoltage of 2.5V in the lower range, the noise would need to be improved.

6.2.3 Optical Cross Talk

The Optical Cross Talk should be linear and independent from temperature. This is confirmed for HPK S12642. Minor diviations from that are probably due to slight errors in the breakdown-voltage calculation from the gain regression line. The diviation of 30° C and 35° C below an

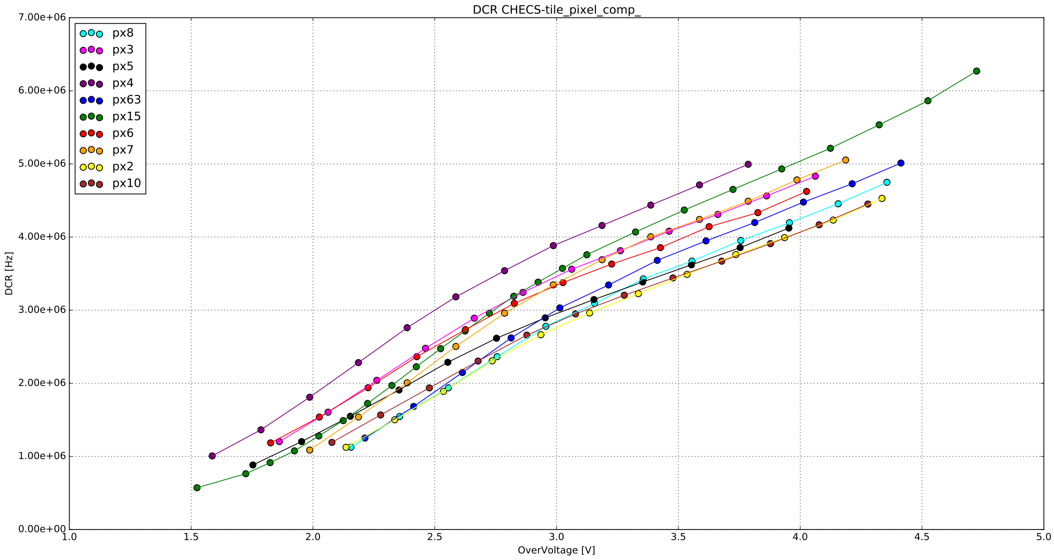

Figure 28:

over-voltage of 2V stems from the way the gain regression line is used to calculate both Dark Count Rate and Optical Cross Talk. At higher temperatures the lower voltage range is dominated by noise, so using the gain regression line to calculate the Optical Cross Talk at those low voltages leads to the visible effect of the first few datapoints of 30° C and 35° C. The deviations between the different groups results at 25° C (green) are caused by 4 major contributions. Firstly the difference in the tested device. While I take measurements on 4 3mm^2 pixels electricaly tied together, the way the device will later be implemented into CHEC-S, the groups in the US and Hamamatsu Photonics are likely to run tests on 1 3mm^2 pixel only. Secondly I suspect a slight difference in amplification and shaping electronics. The measurements I conducted as well as the measurements of Leicester are done with the same shaper and buffer configuration. The difference here is, thirdly, my measurements are done with dark counts only, while measurements from other groups are conducted with a pulsed light source and reading out timed windows. This causes the results from Leicester to be difficult to compare against, their surface temperature of the SiPM is likely much higher than 25° C, and thus, a misinterpreted breakdown-voltage at 25° C causes a shift of the Optical Cross Talk to the right. Lastly the difference in actual data taking and analysis procedure must be mentioned, also this is only of minor concern, as we will see with other measured devices.

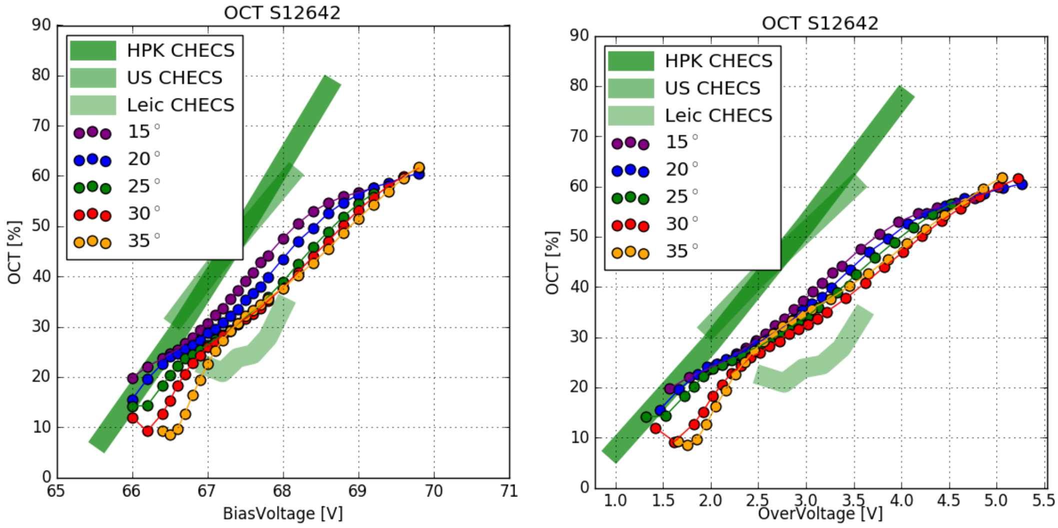

Figure 29: Dark Count Rate of the HPK S12642 pixel, plotted against over- , bias-voltage and temperature.

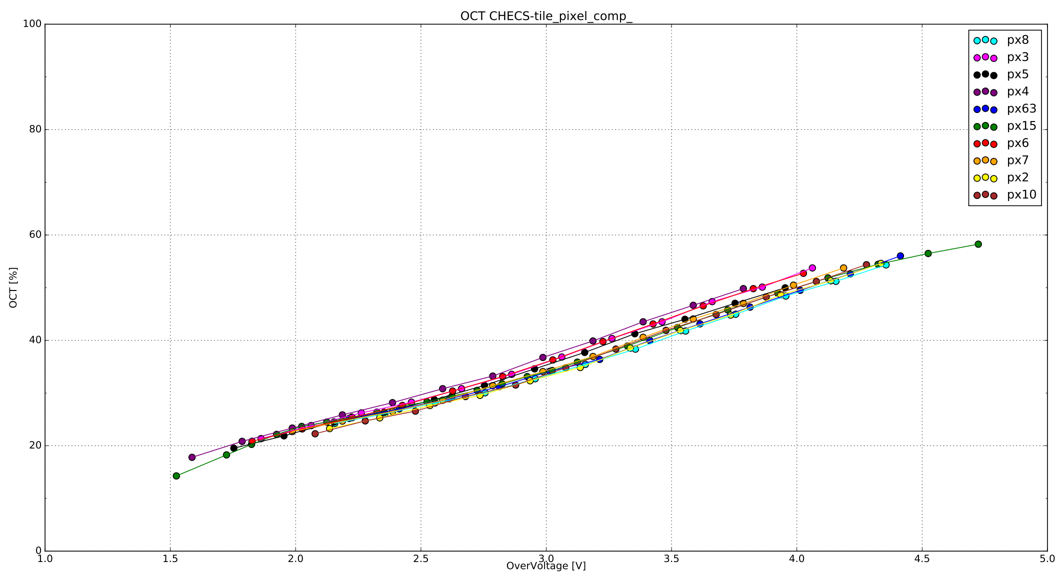

Figure 30:

6.3 Hamamatsu LCT5 50μm 6mm

The Silicon Photomultiplier designated HPK S13360 6050CS is an LCT5, meaning Low Cross Talk 5th iteration device from Hamamatsu Photonics. It is one of the most promising candidates for later usage in CHEC-S. It has a pixelsize of 6mm^2 consisting of 14400 cells with a cellsize of 50μm. The present device and its similar iterations are the first to incorporate trenches bordering each cell, effectively insulating the cells and reducing the prompt Optical Cross Talk very effectively. Tests are done with a single pixel only, in contrast to measurements done on S12642. It is mounted on a ceramic chip and coated with a silicon resin that is UV-transparent. Wire bonds supply the electrical contact. A similar, but not tested, device from the same generation uses through-silicon-via (TSV) technology, realising electrical connection through the silicon bulk, allowing a tighter fit of the cells, with minimal dead-space. The layout of the single pixle test device made external amplification necessary. I used a MiniCircuits PreAMP, which was supplied with 13V during this test. Shaping of the pulse is conducted by a CHEC-S shaper, modified to fit the new unshaped pulse. Even though the pulse shape fig(**??**) makes the pulses appear much harder to analyse, due to the possibility of events occuring during the ringing window. This assumption proved untrue, due to the devices low Dark Count Rate and Optical Cross Talk.

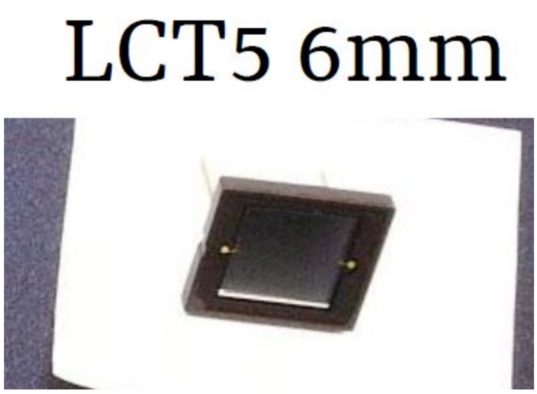

Figure 31: HPK S13360 6050CS pixel

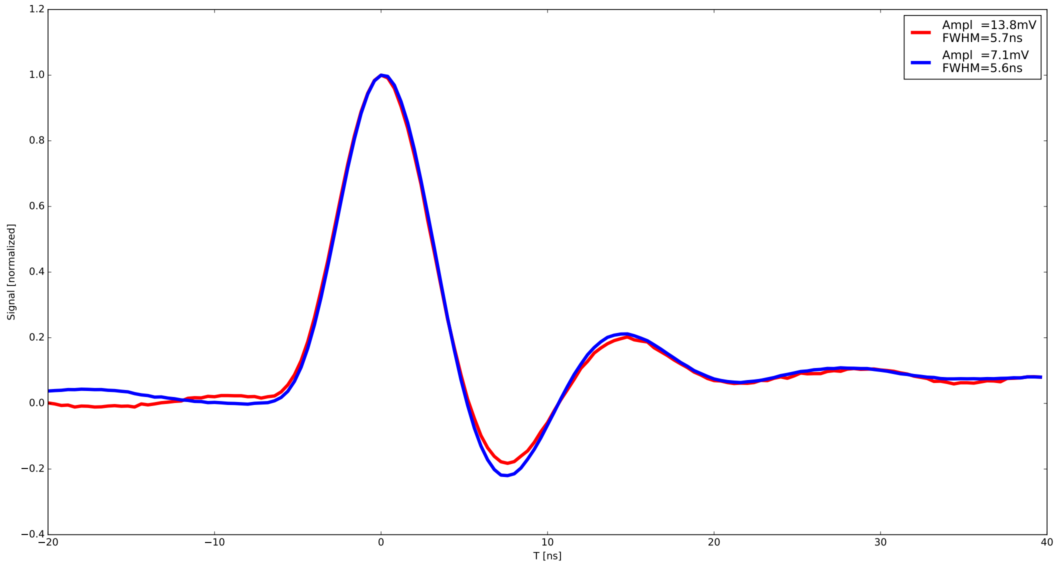

Figure 32: The average pulse shape of the 1photoelectron in blue and the 2photoelectron pulse in red of HPK S13360 6050CS at 25° C and at point of operation. Both pulses have a FWHM of around 5ns and ring for approximately 20ns with an undershoot of 20%.

6.3.1 Gain

The gain of the LCT5 50μm 6mm device is clearly linear with some minor outliers at 30°C. The same effect as with S12642 is visible at 35°C, again counting noise peaks as 1p.e. peaks, resulting in an apparent lowering of the gain and the slope changing over into a plateau. In Figure(**??**)(left) the gain is shown, plotted against over-voltage. It is still dependant on temperature, but due to reliable breakdown-voltage calculation, the spread is much smaller than, if plotted against bias-voltage. The same conversion is done to transform relative gain into an absolute gain with sensible units. When parametrized with over-voltage, the gain is essentially temperature independent.

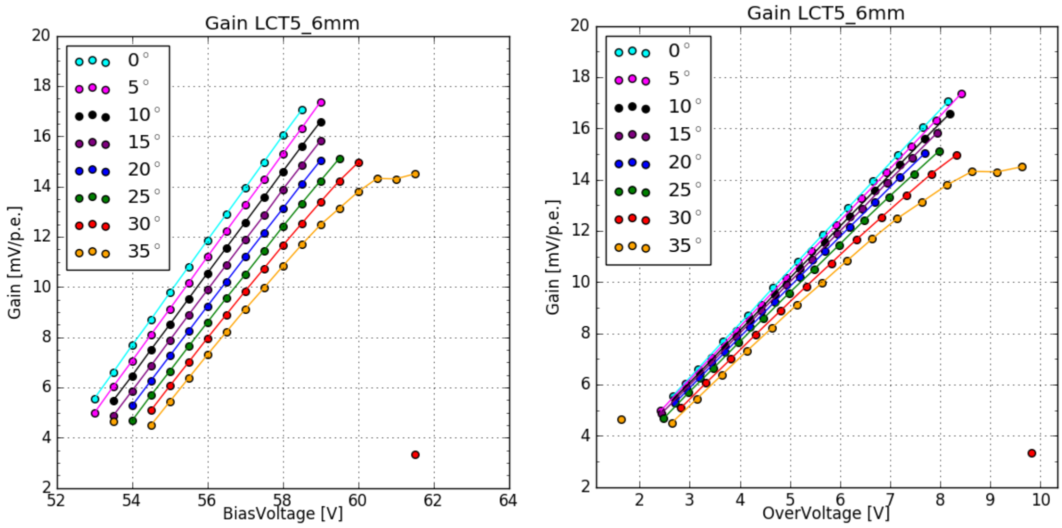

Figure 33: Gain of the HPK S13360 pixel, plotted against over- , bias-voltage and temperature.

6.3.2 Dark Count Rate

The Dark Count Rate of two similar HPK S13360 devices is shown in Figure(**??**). The bars show the difference between the two devices, the results of one device is used as a reference, while the deviation is illustrated with the filled bar. The Dark Count Rate of HPK S13360 followes the expected behaviour, mostly linear in the significant range and rising with increasing temperature. Below an over-voltage of 2.5V my analysis struggles, I suspect the gain to be to low for my analysis to pick up pulses. Thus the regression line calculation is unreliable in this range. The turnup at high over-voltages is most prominent at 0°C(teal) after an over-voltage of 9V. This is also the point where the Optical Cross Talk rises very rapidly.

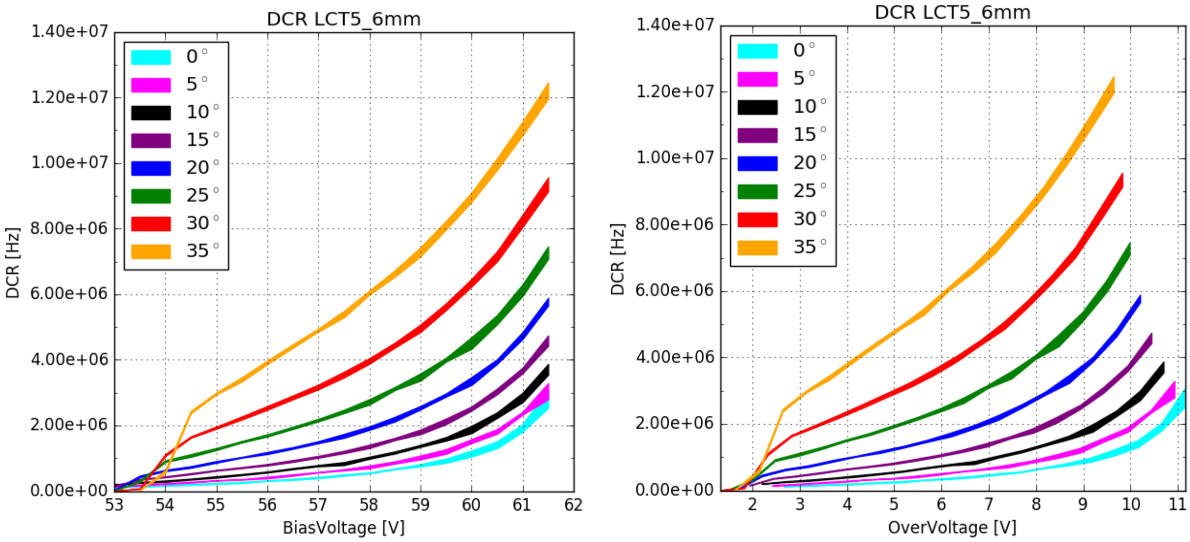

Figure 34: Dark Count Rate of the HPK S13360 pixel, plotted against over- , bias-voltage and temperature.

6.3.3 Optical Cross Talk

Compared to measurements on HPK S13360 done at the Nagoya University Japan **??** (faded green bar), I see a very strong correlation of the Optical Cross Talk in the over-voltage range between 2.5V and 9V. The Optical Cross Talk in this range is linear and independent from temperature, with minor deviations attributed to the breakdown-voltage calculation from the regression line, causing the horizontal shift. In contrast to my technique, using only dark counts, the measurements at Nagoya University followed a pulsed light source approach, reading out a time-window after the laser incident. This could have consequences, since Optical Cross talk with a large delay time could be missed. Deviations below an over-voltage of 2.5V are expected, they are very likely caused by the regression line calculation being unreliable in this range due to the analysis method struggling to pick up pulses using dark counts. Above an over-voltage of 9V, which is also the point of the turnup of the Dark Count Rate, the Optical Cross Talk is no longer linear and the deviation from the results of Nagoya University increase very rapidly. I suspect the rapid increase in both Dark Count Rate and Optical Cross Talk to be caused by the over-voltage reaching ranges, where interpretation of noise as a 1p.e. pulse becomes more likely. This, joint together with the usage of the Mini-Circuits amplifier supplied with 13V, makes false interpretation of noise as pulses even more likely. I suspect these two reasons in conjunction are responsible for both, the sudden rise of the Dark Count Rate as well as the deviation of the Optical Cross Talk from linearity and the results of Nagoya University, above over-voltages around 9V. In summary, the correlation between the two measurements, conducted by two different methods of data acquisition and analysis, is evident.

The S13360 series is the first to incorpore physical barriers, called trenches, effectively insulating the cells from each other. This drastically reduces the promt cross-talk, while increasing the percentage the delayed cross-talk contributes to the overall cross-talk shown. This could also be the reason for the upturn compared to data from the University of Nagoya, at higher over-voltages the contribution from delayed cross-talk is higher. With the trenches effectively reducing the prompt cross-talk and the difference in analysis, the effect could be partially explanied by increased contribution of the delayed cross-talk. More on this subject in chapter **??**.

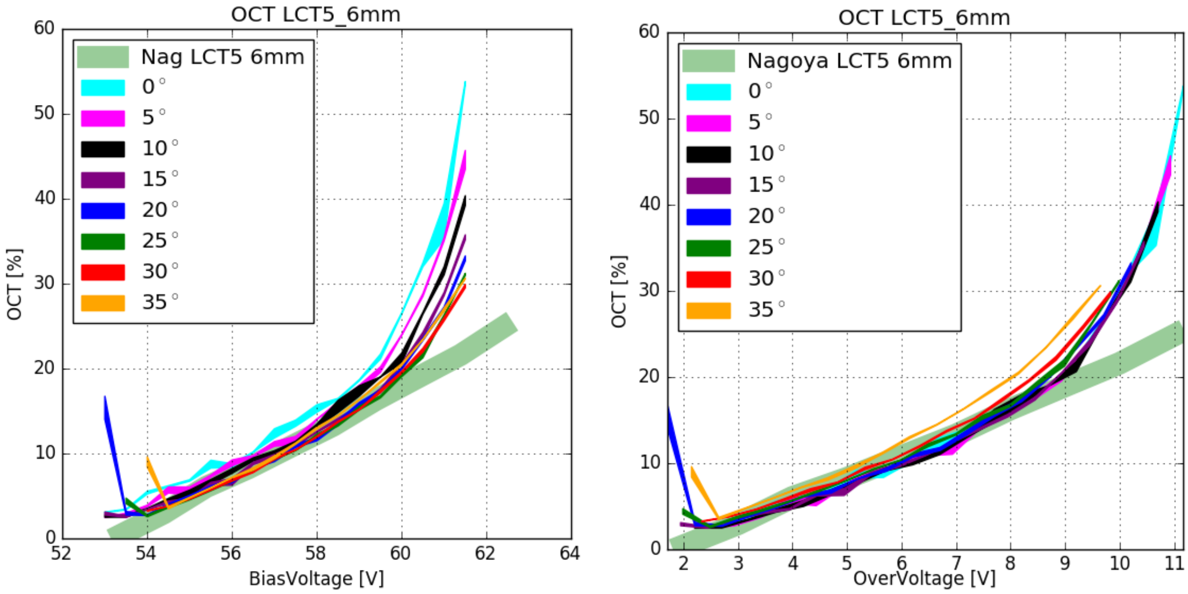

Figure 35: Optical Cross Talk of the HPK S13360 pixel, plotted against over- , bias-voltage and temperature.

6.4 Hamamatsu LCT5 75μm 7mm

Figure 36: HPK LCT5 7mm pixel

XXXXXXXXXXXX is a larger LCT5 prototype Silicon Photomultiplier of the same design as S13360-6050CS. With an increase in cellsize to 75μm, the device gains a higher fill-factor than 50μm devices. The pixelarea is also expanded to 6.915mm^2, which will result in a larger FoV of GCT, see chapter (list of devices etc) !(maybe tom armstrongs simulations)!. Since it is a prototype device, there is limited data from datasheets. The ID number suggests, that it is also a wire-bond device with a UV-transparent silicon-resin coating. It is also a single pixel test device, so external amplification is necessary. I used the same minicircuits PreAMP Sn XXXXX, supplied with 8V during this test. The signal is also shaped by a differently modified CHEC-S shaper, which results in a pulse shape similar to S12642, but with a much lower amplitude.

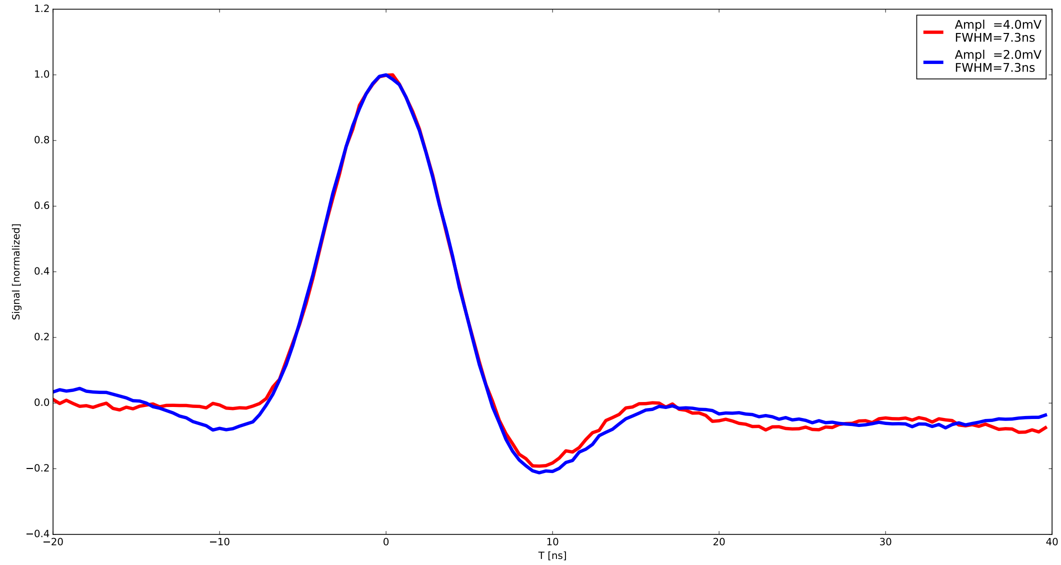

Figure 37: The average pulse shape of the 1photoelectron in blue and the 2photoelectron pulse in red of HPK LCT5 7mm at 25° C and at point of operation. Both pulses have a FWHM of around 7ns and an undershoot of 20%, with no ringing.

6.4.1 Gain

Figure(**??**) shows the gain of the LCT5 7mm device. Two sets of measurements are done for 25°C to extend the measured range. The first set of measurements covers the lower over-voltage range, where the low gain makes external amplification necessary. The same MiniCircuits PreAMP supplied with 8V was used during this test. I chose the lowest possible amplification of the PreAMP, so that reaching the point of saturation of the oscilloscope input is as late as possible as the over-voltage rises. Saturation of the oscilloscope occurs due to the possibility of generating very large p.e. (>10p.e.) events at the higher over-voltages, which are saturating the input. Joint together, the LCT5 7mm device and the MiniCircuits PreAMP at 8V reach this point at an over-voltage of ∼6V. In Figure(**??**) the results from the lower range measurement are displayed as the lower-range green line extending between an over-voltage of 1.6V to 5.4V.

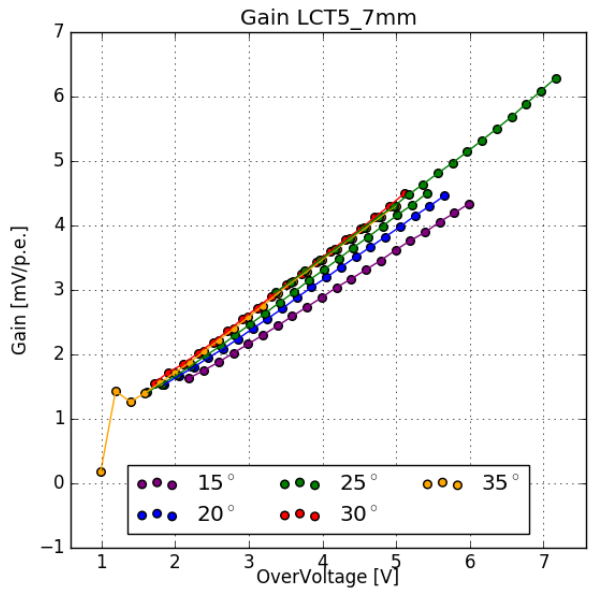

Figure 38: Gain of the HPK LCT5 7mm pixel

The configuration for the second test removes the PreAMP from the setup, which makes the lower over-voltage range unaccesible, but extends the range to higher over-voltages. This configuration reaches the point of saturation at an over-voltage of ∼8V. The higher range measurement results are displayed as the second green line (25°C) extending from 3.4V to 7.2V over-voltage in Figure(**??**). There is a clearly visible overlap of the two measurements between ∼3.4V and ∼5.4V . It also seems, that the gain dependency on temperature is reversed. While for all other devices, the gain lowers with rising temperatures, the LCT5 7mm device seems to show inversed behaviour. This inverse behaviour is caused by the calculation of the breakdown-voltage from the gain-regression line, with this and the bias-voltage, the over-voltage is calculated, causing a horizontal shift. Plotting the gain versus bias-voltage shows the expected behaviour.

6.4.2 Dark Count Rate

The behaviour of the Dark Count Rate of the HPK LCT5 7mm device is shown in Figure(**??**) and is as expected, in contrast to the behaviour of the gain of LCT5 7mm, as discussed in section **??**. It follows a linear progression in the relevant range and increases with rising temperature. I suspect the over-voltage range above ∼2.5V to be relevant. The extended range measurement at

25°C confirms this behaviour. LCT5 7mm shows a linear Dark Count Rate over an over-voltage range of 4V. The faded green bar in Figure(**??**) shows results from measurements undertaken by the Department of Physics and Astronomy at the University of Catania. Those measurements were conducted on the exact same device, which is an important point, but with a different method of data acquisition and data analysis. Analysis techniques are discussed in chaper **??**. The correlation between the two experiments is evident, although there is differences in the acyquisition and analysis process. This is further proof for the relevancy of my analysis.

6.4.3 Optical Cross Talk

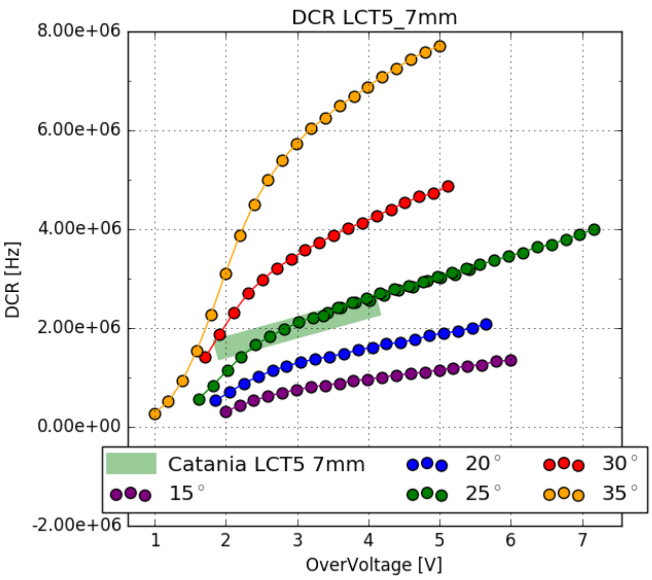

Figure 39: Dark Count Rate of the HPK LCT5 7mm pixel

The Optical Cross Talk is expected to be linear and independent from temperature. This is the case in the, in section **??** established, relevant over-voltage range of above ∼2.5V. Minor deviations are attributed to the calculation of the breakdown-voltage from the gain-regression line. The over-voltage is calculated from the former and the supplied bias-voltage, which in turn causes a slight horizontal shift. With that, comparing my results to the measurements from the University of Catania shows a strong correlation. Keeping in mind, that the process of data acquisition and analysis is different for both measurements further proofs my analysis valid.

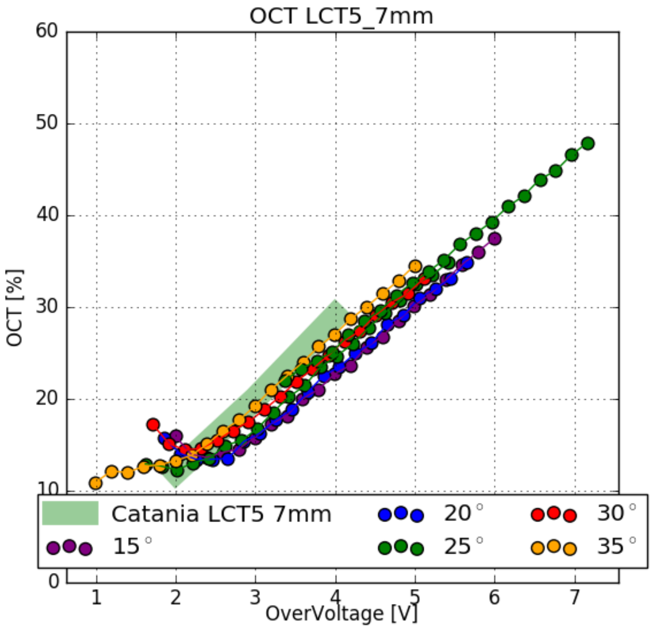

Figure 40: Dark Count Rate of the HPK LCT5 7mm pixel

6.5 Hamamatsu LVR 50μm 6mm

The Silicon Photomultiplier by Hamamatsu Photonics with the designation 6050HWB-LVR-LCT is a special prototype of the LCT5 design. LVR is an abreviation of Low Voltage Range, meaning the device is meant to be operated at much lower operation voltages than other LCT5 devices. It has the same physical size as an LCT5 50μm 6mm device (S13360 chapter **??**), a pixelsize of 6mm pixel with a cellsize of 50μm. The recommended point of operation however is ~15V below that of the S13360 device, specifically at 40.2V(LVR) instead of 54.7V (S13360). The unshaped signal is similar to other LCT5 devices, therefore using the same modified CHEC-S shaper is feasible in this case. After that the signal is amplified with the same MiniCircuits PreAMP supplied with 8.5V.

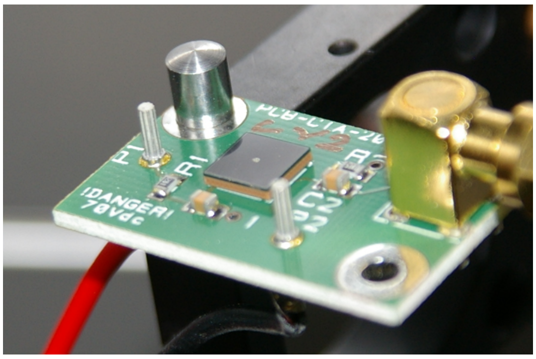

Figure 41: HPK LVR 6mm pixel

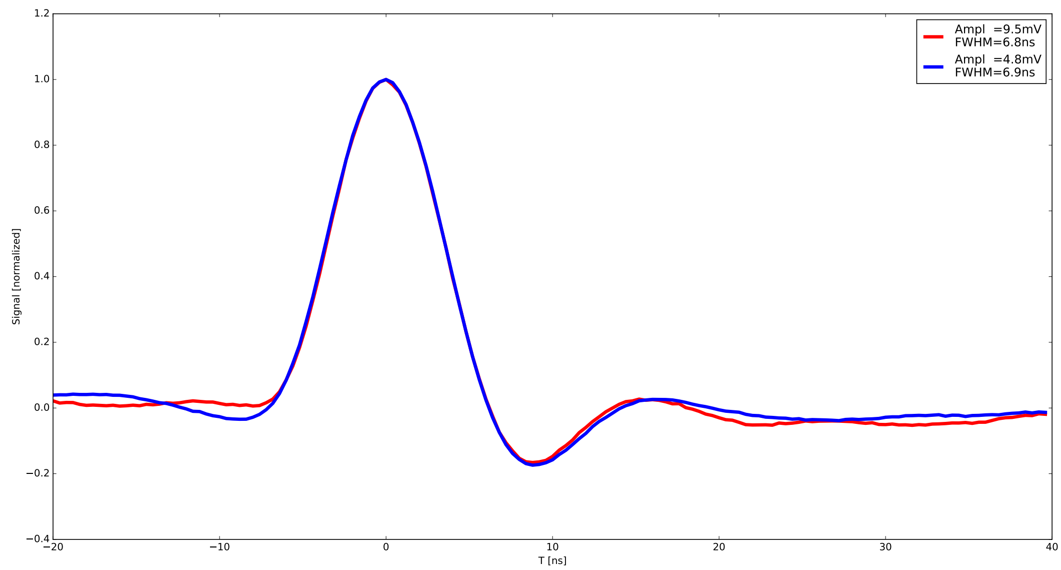

Figure 42: The average pulse shape of the 1photoelectron in blue and the 2photoelectron pulse in red of HPK LVR 6mm at 25° C and at point of operation. Both pulses have a FWHM of around 7ns and an undershoot of 20%, with no ringing.

6.5.1 Gain

Figure(**??**)(left) shows the gain of the LVR 6mm device. It is, as expected, linear over a long range. The flattening of the slope to a plateau shape in the lower over-voltage range, is caused by the analysis being unable to identify peaks lower than the set threshold. Only taking into account the linear region, limits the range, where the results are relevant to an over-voltage range of ∼2.5V. Saturation of the oscilloscope in this range is not visible, but a check with a more expanded range revealed, that the point of saturation of the oscilloscope is at an over-voltage of ∼5V. The apparent overlap of the gain, when plotted against over-voltage, is based on the calculation of the breakdown-voltage being very reliable due to the large linear range. Plotted versus bias-voltage Figure(**??**)(right) the expected behaviour of the gain, lowering with increasing temperature, is visible.

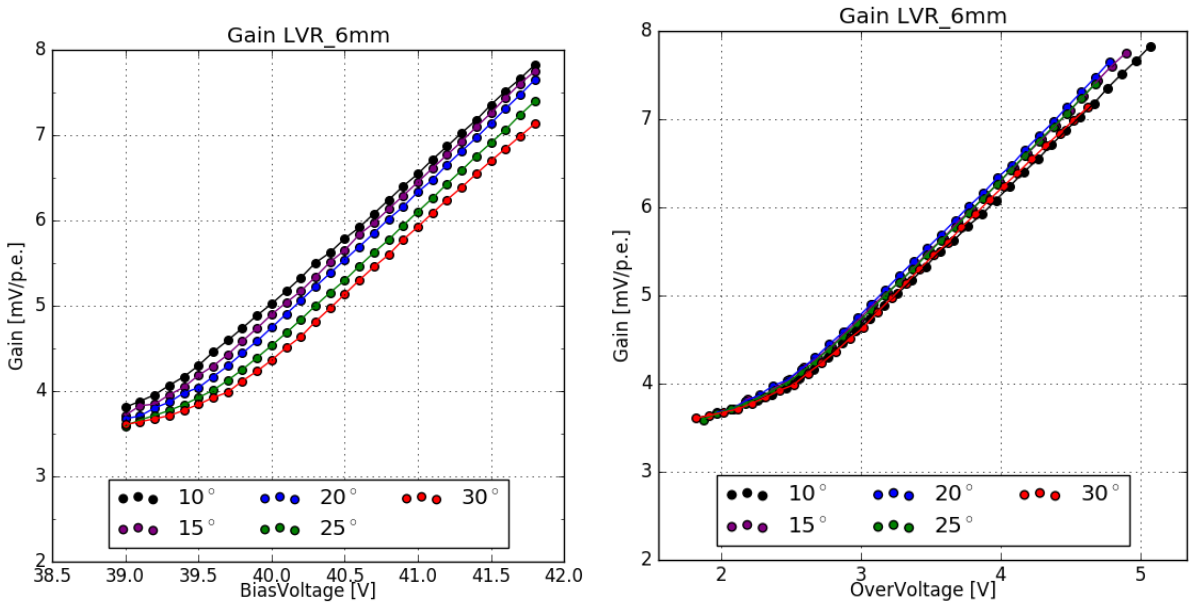

Figure 43: Gain of the HPK LVR 6mm pixel

6.5.2 Dark Count Rate and Optical Cross Talk

The Dark Count Rate, taking into account only the relevant over-voltage range of >∼2.5V seems to correlate with the results form the University of Nagoya. But the resulting Optical Cross Talk is very high compared to results from the University of Nagoya, which also cover a much wider range. Only taking into account the previoulsy established relevant over-voltage range of >∼2.5V, the resulting Optical Corss Talk is a factor of 2 higher. This uncertainty is a contrast to results from previous devices, where strong correlations between different groups and measurement techniques are evident. I suspect, that the device examined by me and the device present at Nagoya University are slightly different prototypes.

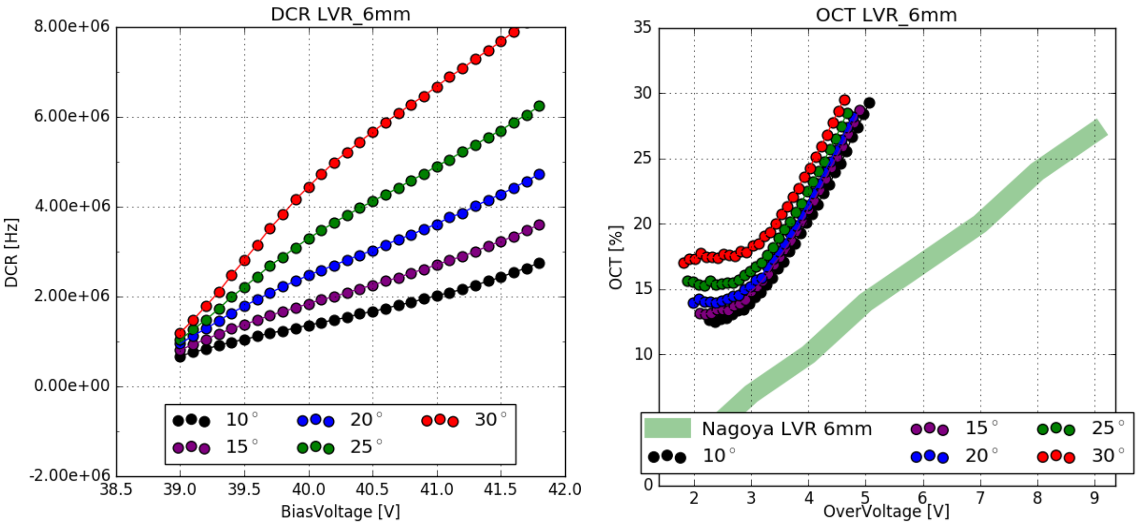

Figure 44: Dark Count Rate and Optical Cross Talk of the HPK LVR 6mm pixel

6.6 SensL FJ60035 6mm 35μm

The Silicon Photomultiplier by SensL with the designation FJ-60035 is also a candidate device for use in CHEC-S. It is also a 6mm device, but with a much smaller cellsize of 35μm, using the TSV technology, so there are no wire-bonds present. This results in 22292 cells on a single pixel with a fill-factor of 75% . It is coated with plain glass. The recommended point of operation is around 30V bias-voltage, lower even than that of the HPK LVR prototypes. The device is, by the manufacturer, pre-mounted on a printed circuit board, called a test array. This test array contains a fast output, that directly couples to the cells, and a slow output, conventionally read out via the quench resistor. For the conducted tests, I used the fast output amplified with the MiniCircuits PreAMP supplied with 12V. The SensL device was the first device measured, therefore the analysis procedure used was an older iteration compared to the procedure for the Hamamatsu devices.

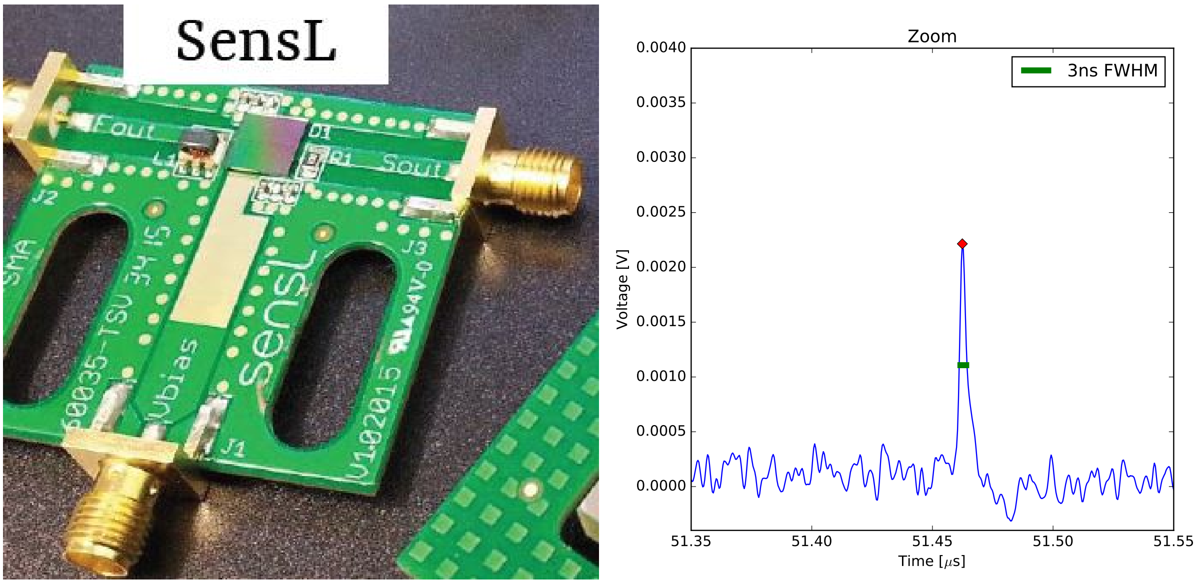

Figure 45: SensL Test Array and pulse shape at bias-voltage = 29V0

6.6.1 Gain

Evaluating the SensL pulse area spectra shows the 1 p.e. position and Δp.e. overlapping, so using the older analysis iteration introduced no error when evaluating the gain of the SensL device. It is clearly linear over a wide temperature range from -5°C to 35°C over an over-voltage ranging from 2V up to 8V. When plotted versus over-voltage the spread of the gain is even tighter, while still following the expected behaviour of decreasing with increasing temperature.

6.6.2 Dark Count Rate and Optical Cross Talk

The Dark Count Rate also shows the expected behaviour. At very low temperatures the changes in rate over the over-voltage range is minimal. Increasing the temperature shows a rapid in-

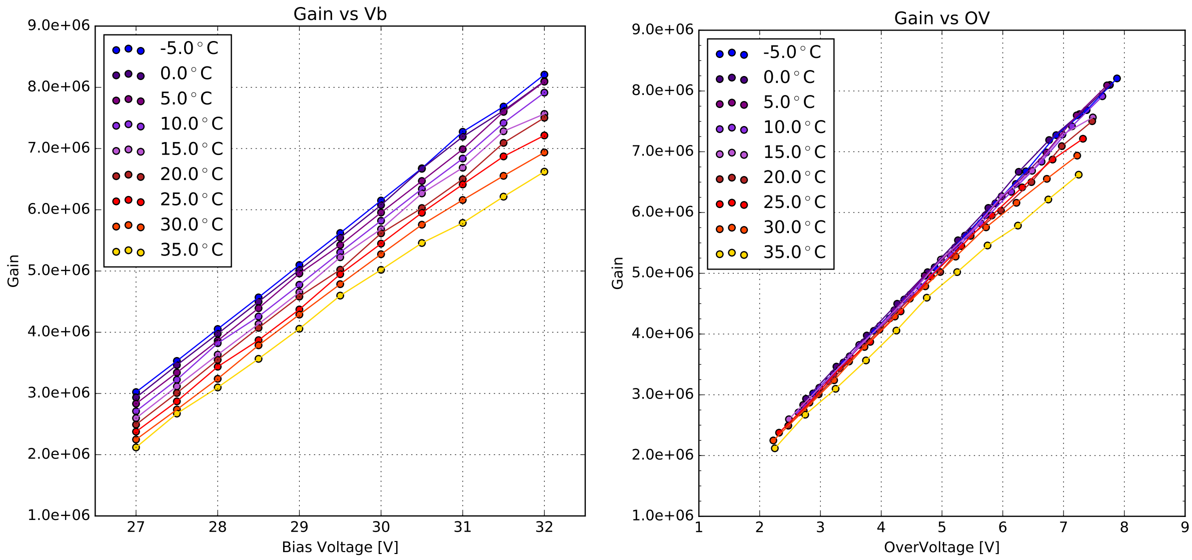

Figure 46: Gain of the SensL FJ-60035 test array

crease in thermally induced dark counts. The Optical Cross Talk on the other hand is independent of the device temperature, also as expected.

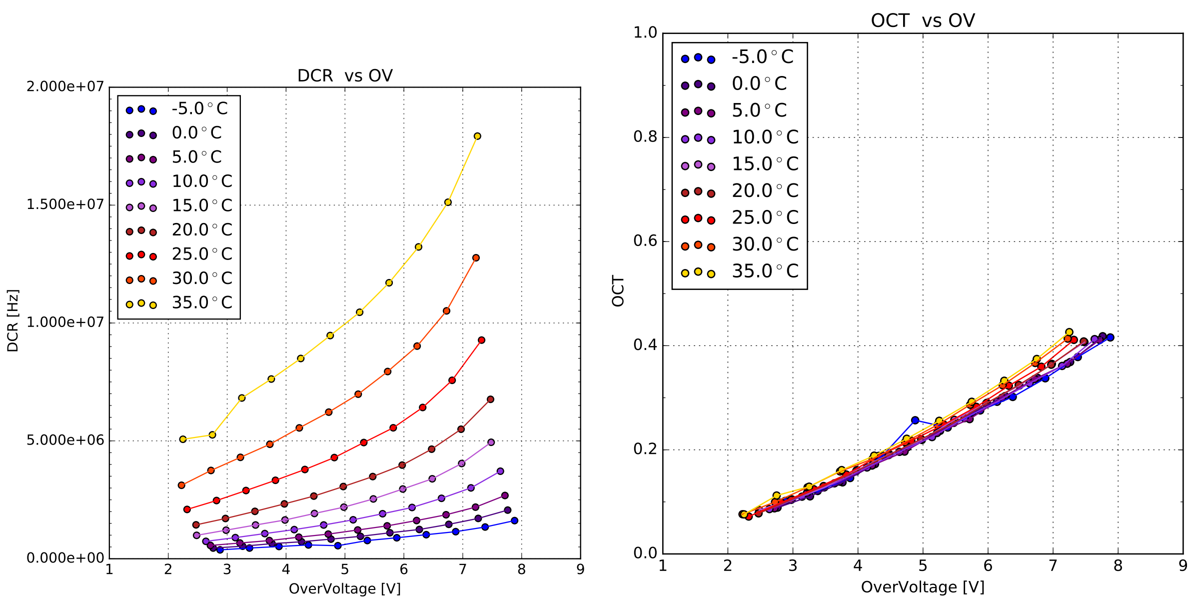

Figure 47: Dark Count Rate and Optical Cross Talk of the SensL FJ-60035 test array

7 Comparison

A comparison of the performance of all devices is the significant step for choosing the Silicon Photomultiplier later to be used in CHEC-S. In order to do this, all measured characteristics are compared versus over-voltage. Operation of the CHEC-S camera in GCT will come down to a decision between two operational points. The first point will be marked by an Optical Cross Talk of under 15%. Every other attribute of the Silicon Photomultiplier at this over-voltage is then compared. This point will trade off precision for efficiency, a lower Optical Cross Talk makes real event detection easier, on the other hand, a lower Photon Detection Efficiency may forfeit a lot of potential data.
The second point of operation is marked at the highest achievable Photon Detection Efficiency. My conducted measurements do not involve this, other groups are comissioned to determine the point of highest Photon Detection Efficiency, in other conducted measurements, that are comparable **??**. This point will assure the highest detection of event photons, but will trade that for an increase in detector noise, due to the higher Dark Count Rate and more importantly Optical Cross Talk.
Comparing results to other groups is shown in Figure (**??**), using different experimental setups and procedures and therefore also entirely different analysis techniques. Comparing against results from the University of Leicester, the University of Nagoya and the University of Catania, all of which are conducting fixed window readout of the SiPM after an expected light-pulse from a flasher-LED or pulsed laser.

7.1 Dark Count Rate

Comparing the Dark Count Rate of the measured devices and results from the other groups is shown in Figure **??**. The differences in analysis procedure will only have a slight impact on the presumed Dark Count Rate, since all experiments record dark-count events over their respective acquisition time windows. On the other hand, if the readout window is sufficiently small, events originating from afterpulsing or delayed crosstalk could be missed. All groups experience the same multi-hit coincidence, meaning a light-event or dark-event coinciding with another, forming a (partial)multi p.e. event.
Missing:
LCT5 7mm to catania
LCT5 LVR to nagoya

7.2 Optical Cross Talk

The comparison of the Optical Cross Talk between the different groups and the results presented in this paper are dependant of the analysis and acquisition procedure. Extended trace analysis,

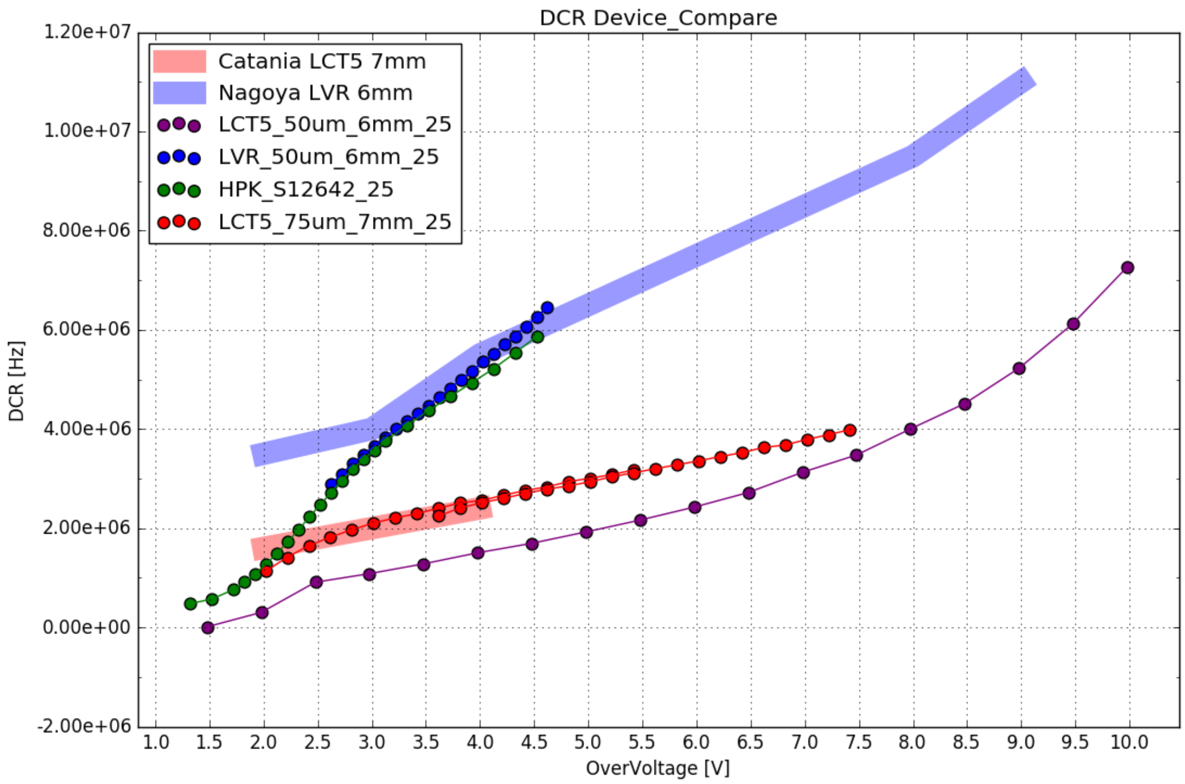

Figure 48: Dark Count Rate comparison of measured devices at 25°C. Description

utilized in this paper captures all aspects of the Optical Cross Talk, prompt and delayed as well as afterpulsing. The procedure of time window analysis, utilized by the groups being compared to, are, due to their limited window, either biased towards the prompt cross talk or in extreme cases, will not be able to capture delayed cross talk or time-delayed afterpulsing at all. Comparing data analysis techniques, for example, at the University of Leicester is therefore a vital step. Their approach utilizes a pulsed laser as light sources and involves no cooling of the SiPM tile. The waveforms are extracted from the scope and a small time window is defined from the known time position window of the incident pulse to search for peaks, find their value and generate a histogram. To the pulse area histogram, a model of theoretical model of contributing factors is fitted. This theoretical model simulates values, updating continuosly to find the correct values. Those values are the full set of characteristics of the device in testing, among them: gain curce, breakdown-voltage, OCT, PDE, noise, dynamic range, crosstalk probability.

There are a number of differences in their approach compared to the one utilized in this paper, most important is the time window size. If the window after an incident pulse is too short, data loss is a possibility, depending on the delay time of delayed cross-talk and afterpulsing assisted by traps with long lifetimes. This is a problem, especially with devices of the LCT5 generation implementing physical trenches isolating the cells and effectively reducing the prompt cross-talk, the contribution from the prompt cross-talk to the overall Optical Cross Talk is lowered. For time window analysis with short window times, missing data from delayed cross-talk and afterpulsing, because it will not be recorded yet, would lead to errors in the overall Optical Cross Talk results being lower than expected.

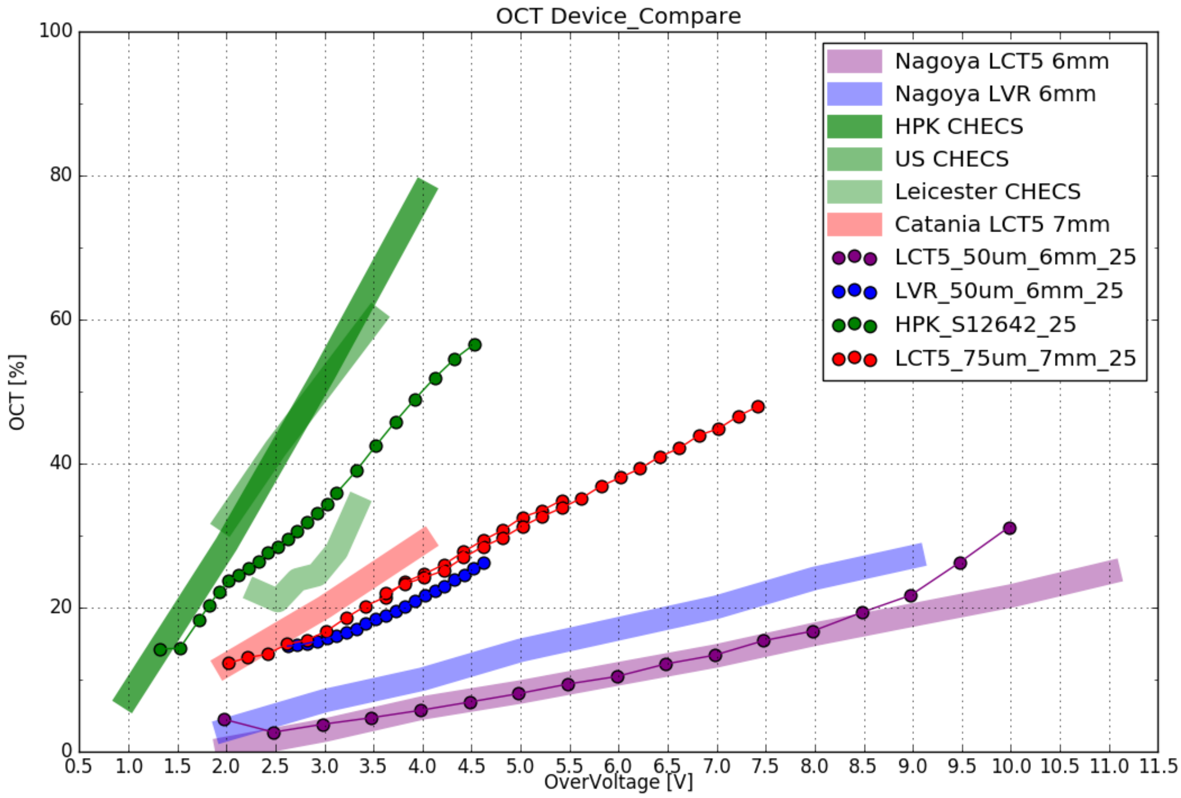

Figure 49: Cross Talk comparison of measured devices at 25°C. Description

This is indeed the case for the S12642 tile in Figure **??** (green). The light green bar below the dotted data presented in this paper shows the results form the University of Leicester indeed being lower. In purple results of the LCT5 S13360 device with physical trenches are shown. Compared to results from the University of Nagoya, there is a prominent upturn at aroung an over-voltage of ∼8V. This could be due to the differences in analysis technique. The University of Nagoya also employs time window analysis. LCT5 posseses lowered prompt cross-talk probability, so the contribution of delayed cross-talk is higher than for S12642. With rising over-voltage the ratio between prompt and delayed cross talk shifts towards a higher contribution from delayed cross-talk. While at lower over-voltages (∼2V) contributions are mostly equal, at high over-voltages (∼8V) the contribution of delayed cross-talk is above 80%, probably due to higher penetration depth and avalanche probalility.

Missing:

LCT5 7mm to catania

LCT5 LVR to nagoya

7.3 Photon Detection Efficiency

Since the measurement technique in this paper utilizes only dark counts and aims at giving an understanding of the Optical Cross Talk and temperature dependencys of the different SiPMs proposed, no PDE measurements are possible. The point of operation with the highest PDE is determined by a different group in Japan, at the University of Nagoya. Figure (**??**) shows the current results of their endavors. MORE later

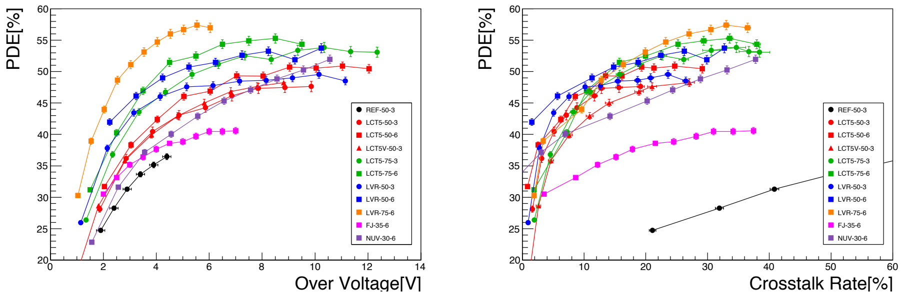

Figure 50: Photon Detection Efficiency Comparison Plots from the University of Nagoya

8 Dark Count Rate recalibration with multi incident probability

9 Prompt and delayed cross talk ratio

10 Conclusion and Outlook

11 Glossary

1. CTA - Cherenkov Telescope Array
2. HPK - Hamamatsu Photonics K.K.

12 Appendix

12.1 BreakdownVoltage

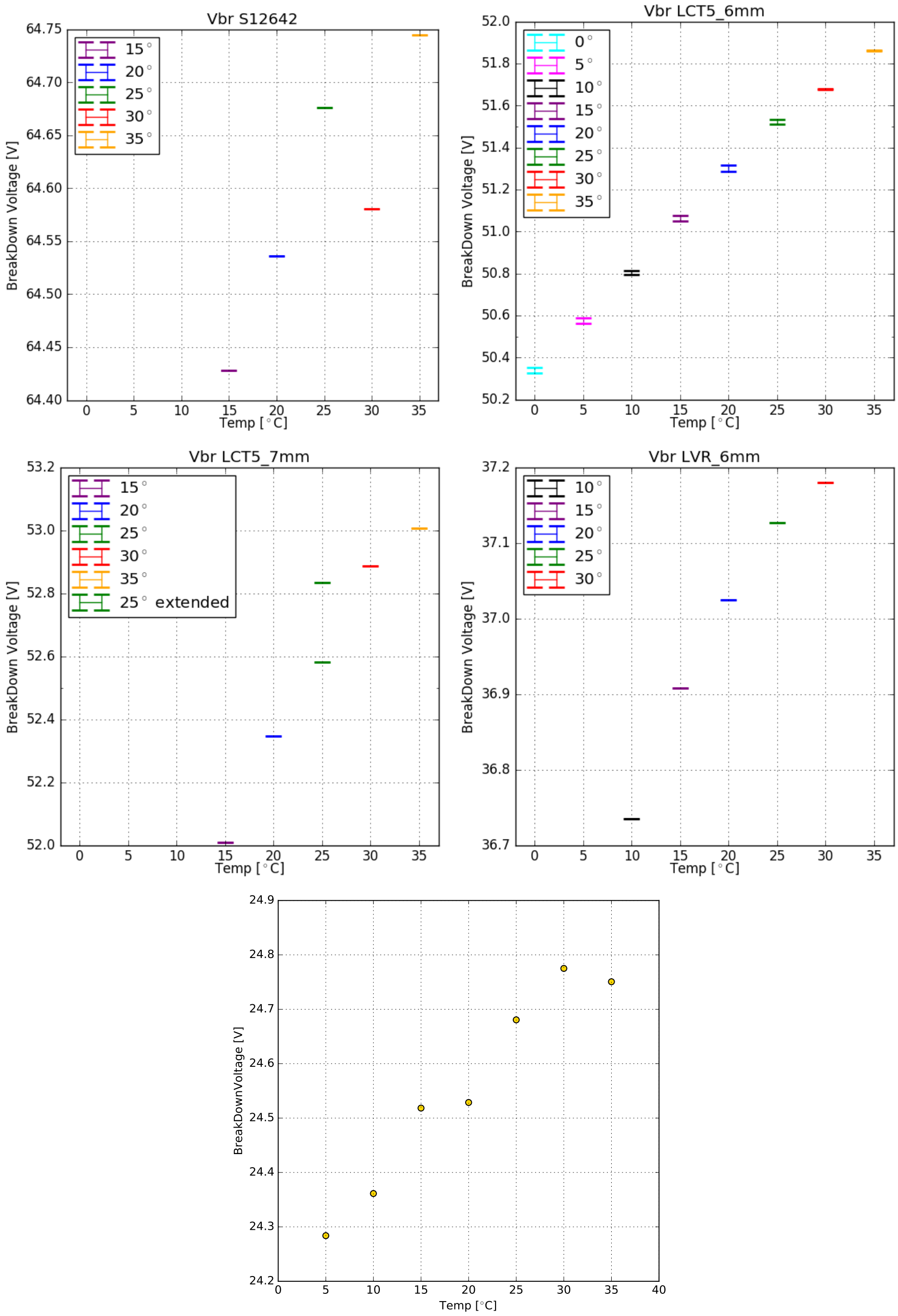
Vbr S12642
BreakDown Voltage [V]
Temp [°C]
15°
20°
25°
30°
35°
Vbr LCT5_6mm
BreakDown Voltage [V]
Temp [°C]
0°
5°
10°
15°
20°
25°
30°
35°
Vbr LCT5_7mm
BreakDown Voltage [V]
Temp [°C]
15°
20°
25°
30°
35°
25° extended
Vbr LVR_6mm
BreakDown Voltage [V]
Temp [°C]
10°
15°
20°
25°
30°
BreakDownVoltage [V]
Temp [°C]

Figure 51:

12.2 HPK S12642 Pixel Comparison versus bias-voltage

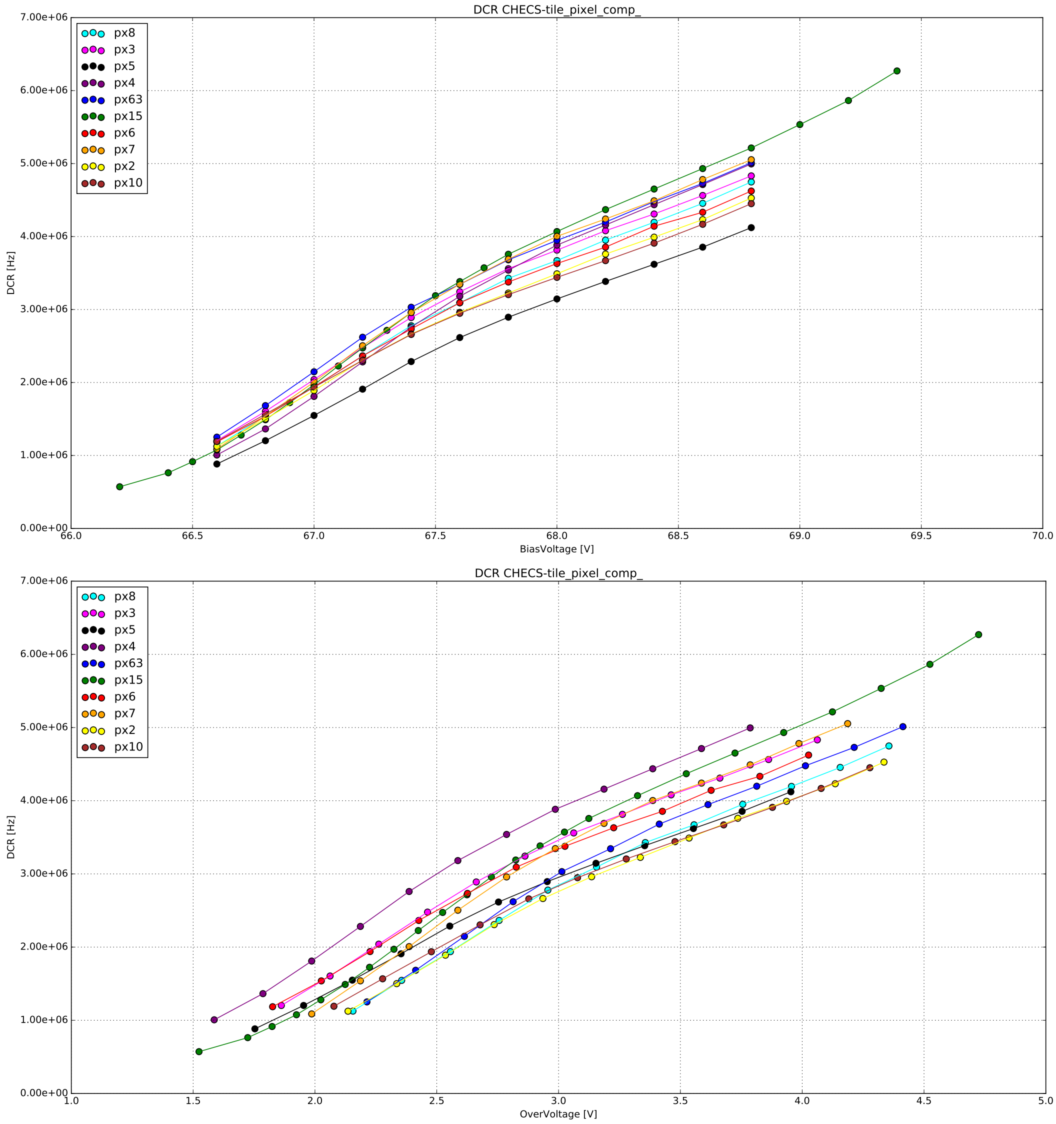

Figure 52:

12.3 Pulse Area Spectra of different integration windows

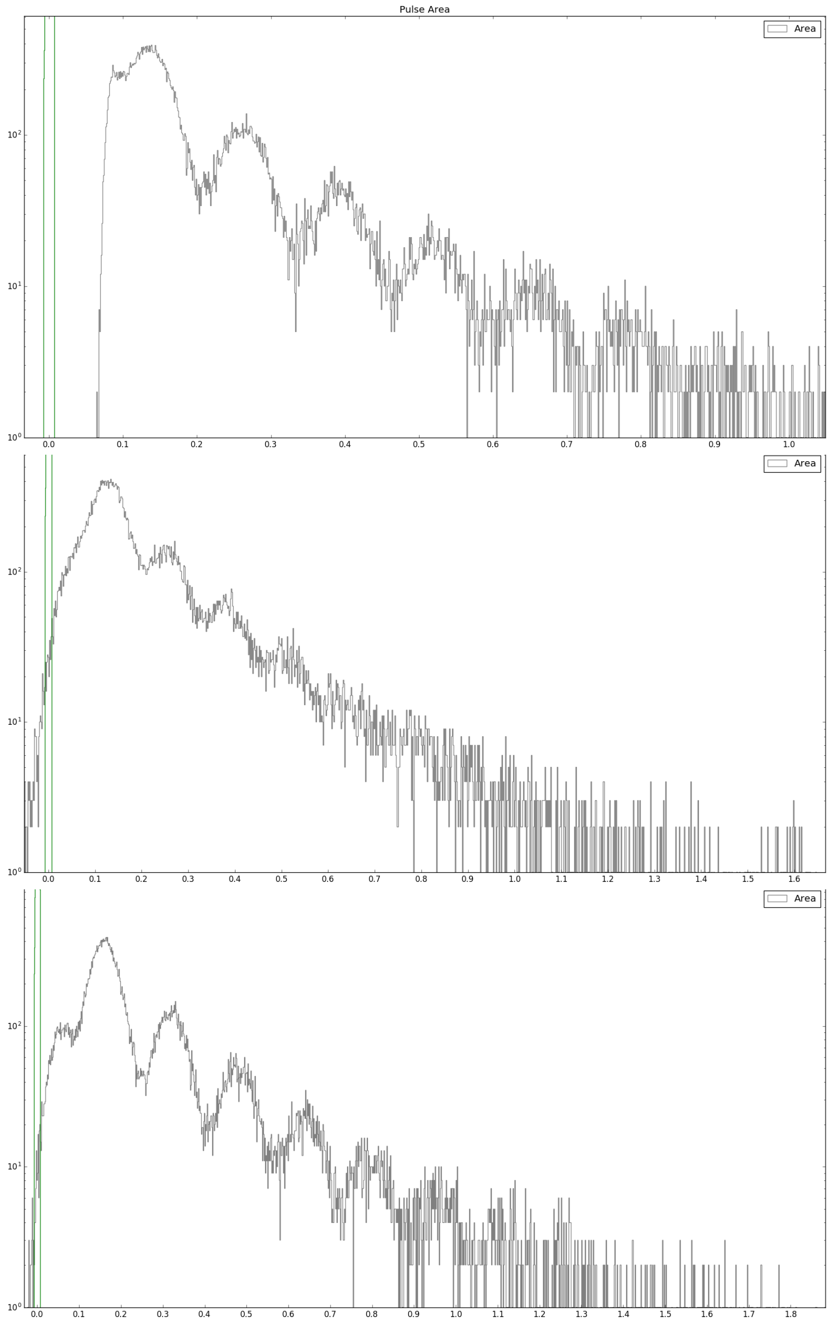

Figure 53: Pulse Area Spectra of 5 left 5 right, 5 left 20 right, 10 left 10 right bins respectively

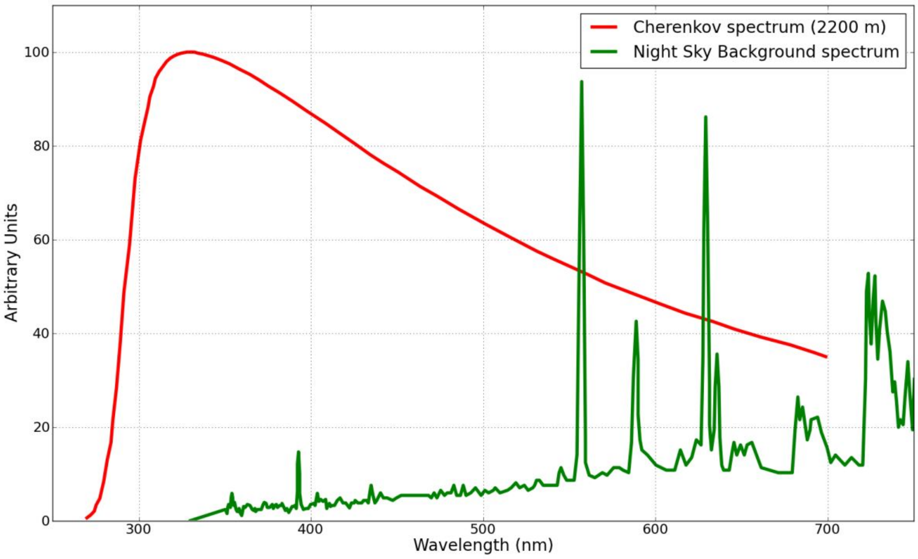

Figure 54: The spectrum of Cherenkov light observed from an extenden air shower at 2200m asl. compared to the expected NSB measured in La Palma. Units on the y-axis are arbitrary because NSB and Cherenkov light vary by different parameters. Image from [??]

12.5 CTA

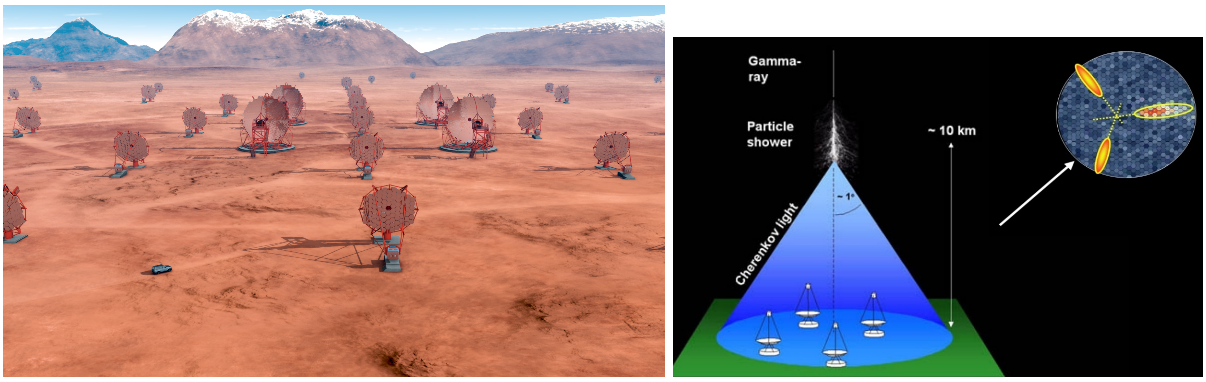

Figure 55: CTA Array and the Shower Path Reconstruction

Figure 56: IACT Projects: MAGIC at the Roque de los Muchachos Observatory on La Palma , one of the Canary Islands. HESS Khomas Highland, Namibia. VERITAS Mount Hopkins, Arizona, USA

13 References

1. Jim Hinton et al. Teraelectronvolt Astronomy Ann. Rev. Astron. Astrophys., 47:523

2. Julien Rousselle et al. Construction of a Schwarzschild-Couder telescope as a candidate for the Cherenkov Telescope Array: status of the optical system

3. CTA Consortium et al. Design Concepts for the Cherenkov Telescope Array

4. Teresa Montaruli et al. The small size telescope projects for the Cherenkov Telescope Array

5. The ASTRONET Infrastructure Roadmap ISBN: 978-3-923524-63-1

6. Jim Hinton et. al Seeing the High-Energy Universe with the Cherenkov Telescope Array Astroparticle Physics 43 (2013) 1-356

7. John Murphy SensL J-Series Silicon Photomultipliers for High-Performance Timing in Nuclear Medicine

8. A. N. Otte et al. Characterization of three high efficient and blue sensitive Silicon photomultipliers

9. http://astro.desy.de/gamma_astronomie/cta/medien/ueber_cta/index_ger.html

10. http://www.ung.si/en/research/laboratory-for-astroparticle-physics/projects/cta/

11. Photosensor Characterization for the Cherenkov Telescope Array: Silicon Photomultiplier versus Multi-Anode Photomultiplier Tube ; arXiv:1308.1390v1 [astro-ph.IM] 6 Aug 2013